Pharmaceutical Sciences. 2026;32(1):130-146
doi:10.34172/PS.026.42494
https://ps.tbzmed.ac.ir/

Original Article

New Morpholine/aryl Carbonyl Thioureas as Antimetastatic Candidates Against Gastric Cancer Cells

Mohsen Sagha[1], Ghazaleh Rahgouy[2], Narges Rajaei[2], Kosar Najafian[2], Jafar Abbasi Shiran[3], Azadeh Aghvami Tehrani[1], Nima Razzaghi-Asl[3*]

[1]Research Laboratory for Embryology and Stem Cells, Department of Anatomical Sciences, School of Medicine, Ardabil University of Medical Sciences, Ardabil, Iran
[2]Student Research Committee, School of Pharmacy, Ardabil University of Medical Sciences, Ardabil, Iran
[3]Department of Medicinal Chemistry, School of Pharmacy, Ardabil University of Medical Sciences, Ardabil, Iran

ARTICLE INFO

Article History:
Received: April 15, 2025
Revised: September 18, 2025
Accepted: October 4, 2025
ePublished: January 5, 2026

Keywords:
AGS, Carbonyl thiourea, Cell migration, Molecular dynamics, Synthesis

Abstract

Background: Inhibition of cancer cell migration is an appropriate strategy for the prevention of metastasis. The purpose of this study was to identify new carbonyl thioureas as inhibitors of gastric cancer cell migration.

Methods: *N1*-(morpholin-4-yl ethyl)/phenyl/aralkyl-*N3*-(thiophene-2-carbonyl)/benzoyl thioureas (**1**-**12**) were synthesized by one-pot two step reaction and assessed for their effect on growth and migration of human adeno gastric stomach (AGS) cell lines through 3-(4,5-dimethylthiazol-2-yl)-2,5-diphenyltetrazolium bromide (MTT) and wound-healing assays. Ras homolog family member A (RhoA) is a guanosine tri-phosphatase (GTPase) oncogenic target with crucial role in gastric cell migration and accordingly molecular docking and molecular dynamics (MD) simulations were performed on RhoA by AutoDock4 and GROningen MAchine for chemical simulations (GROMACS5) software. Drug-likeness scores and pharmacokinetics properties were calculated by MolSoft tool through SwissADME (ADME: absorption, Distribution, Metabolism and Excretion) online server.

Results: All of the compounds relatively inhibited wound-healing process after 24 h, whereas compound **4** exhibited comparable anti-migratory activity to *cis*-platin. Compound **4** might exhibit true migrastatic effect (6.25 µg/mL) without significant cytotoxicity. SwissADME data were indicative of high gastrointestinal (GI) absorption and with the exception of compounds **7** and **9**, all the compounds had lower risk of producing efflux-based resistance. Docking and MD simulations provided stable binding model for top-scored derivative (compound **4**) inside RhoA binding site near to the GTP-binding pocket. All the structural indices were converged in the MD simulations and free energy calculations showed appropriate accommodation inside the RhoA binding site. Bind trajectory analysis revealed no stable intermolecular H-bonds within simulation time and the complex was majorly stabilized through hydrophobic contacts.

Conclusion: The results of the current study suggested that compound **4** may be an appropriate candidate for further development into selective small molecule GTPase inhibitors against gastric cancer metastasis.

Introduction

Gastric cancer has a significant incidence and is still one of the prominent causes of morbidity and mortality led to more than 80000 deaths annually.[1] Gastric cancer is the fourth leading cause of cancer-related deaths globally.[2] Despite prosperous achievements in therapeutic strategies,[3] numerous patients are diagnosed in advanced cancer stages as a result of subtle symptoms and delayed detection.[4] It has been documented that a significant number of resected gastric cancer patients are detected with local relapse or distant metastasis leading to median survival not exceeding than 12 months.[5] Common risk factors associated with gastric cancer include genetics, obesity, smoking, helicobacter pylori infection, high salt intake, low consumption of fruits/vegetables.[6,7] To decrease the incidence of gastric cancer, scientific reports have recommended the contribution of a healthier dietary and lifestyle pattern including physical activity to avoid obesity.[8]

Most frequently utilized treatment approaches are radiation therapy, chemotherapy, targeted therapy and immunotherapy whereas, surgical resection is the most popular therapeutic method for gastric adenocarcinom.[9] Sequential lines of systemic chemotherapy is the major

***Corresponding Author:** Nima Razzaghi-Asl, Emails: n.razzaghi@arums.ac.ir; razzaghinima@gmail.com

treatment approach for the metastatic or advanced gastric cancer.[10] It has been well revealed that the majority of cancer-related deaths is associated with metastasis.[11,12] Metastasis is a complicated heterogeneous process and known as a molecular hallmark of cancer. It is designated by the dissemination of tumor cells toward body tissues through blood/lymphatic vessels.[13] Metastatic dissemination is promoted by cell migration and there is a robust correlation between the mechanisms of cell migration and metastasis progression.[14]

Cancer cell migration is mechanistically associated with the epithelial to mesenchymal transition (EMT) of malignant cells. EMT is an essential mechanism in metastasis and converts epithelial cells into mesenchymal phenotype via loss of apicobasal polarity and intercellular adhesion of epithelial cells.[15,16] EMT allows the solid tumors to be more malignant, with enhanced invasiveness and metastatic activity.[17] Cell migration occurs through a single-cell or a collective dissemination model. In a single-cell migration there are no intercellular connections while collective cell migration occurs as multicellular groups with intercellular connections.[18]

Inhibitors of cancer cell migration have gained a considerable attraction with regard to their anti-metastatic potential.[19] Suppression of cell migration interferes with tumor invasion and angiogenesis as downstream processes and prevents metastasis event.[19] Moreover, migration inhibitors have an advantage over cytostatic agents due to the lower adverse effects and drug resistance.[16] Literature review reveals that *N*-substituted thiourea derivatives exhibit anticancer effects and furthermore[20-23]; *N*1-(2-hydroxy-3-chloro-4-nitro phenyl)-*N*3-benzoyl thiourea derivative was demonstrated to suppress cell migration at concentrations that were inactive for killing SUM Breast Cancer Cell Line Collection (SUM159) cells even after 48 h.[24] It has also been indicated that ruthenium-*N*,*N*-disubstituted-*N*'-acyl thiourea complexes could inhibit migration of cells of the M. D. Anderson Cancer Center-Mammary/Breast (MDA-MB-231) lineage.[25]

Discovery and design of novel drugs are elaborate and time-consuming processes that need considerable financial sources to achieve desirable outcomes. In this context, computer aided drug discovery/design (CADD) or in silico methods are economic strategies that can be used to facilitate the performance of important drug design tasks such as drug-target binding prediction, pharmacophore development, virtual screening. Molecular docking is a well-known structure-based drug design technique the increases the efficiency of the drug discovery strategies through predicting drug-target interactions and comparison of the biological activities to theoretical calculations.[26] Molecular dynamics (MD) is a robust computational approach that is primarily used to determine the stability of ligand-protein complexes via evaluating the dynamic behavior of the molecules as a function of time.[27] Pharmacokinetics issues that are designated by ADME (Absorption, distribution, metabolism and excretion) are equally important in the identification and selection of drug candidates since they are determinant in achievement of a typical drug or ligand to its appropriate molecular target in vivo.[28] Due to their importance, in silico ADME prediction methods are undisputable part of CADD studies.

With regard to our previous interests in the effect of *N3*-substituted-*N1*-aryl/alkyl thioureas on adeno gastric stomach (AGS) cell migration behavior,[29] the purpose of this study is the synthesis of a series of *N1*-(morpholin-4-yl ethyl)/phenyl/aralkyl-*N3*-(thiophene-2-carbonyl)/benzoyl thioureas (**1**-**12**) and determine their effects on the growth and migratory behavior of AGS gastric cancer cells. It is also aimed at the in silico ADME and drug-likeness analysis of synthetic carbonyl thioureas alongside a sequential docking and MD simulations to obtain stable binding model for a top-scored migration inhibitor. For this purpose, *Ras homolog family member A* (RhoA) binding site was computationally targeted since it is an important guanosine tri-phosphatase (GTPase) that is has been documented as oncogenic target in migration, metastasis and progression of gastric cancer cells.[30,31]

Materials and Methods

Chemistry

All the chemical reagents and solvents were purchased from Sigma-Aldrich (India) company and used without purification. Melting points of the products were determined by an Electro thermal type 9200 MP apparatus (England) and uncorrected. Infra-Red (IR) spectra were obtained by a Perkin Elmer-400 Fourier transform-IR (FT-IR) spectrophotometer (England). Proton nuclear magnetic resonance (^{1}H-NMR) and carbon nuclear magnetic resonance (^{13}C-NMR) spectra were recorded on a Bruker DRX400 spectrometer (400 MHz).

*General Procedure for the Synthesis of N1-Phenyl/Aralkyl-N3-(Thiophene-2-Carbonyl) Thioureas (**1-6**)*

To a KSCN (1 mmol) in acetonitrile (15 mL), thiophene-2-carbonyl)/benzoyl chloride (1 mmol) was added. The reaction mixture was stirred for 1 h at room temperature. After appearance of the precipitate, corresponding amine (1 mmol) and triethylamine (3 drops) were added slowly into the solution and heated (40 °C) for 24 h. The progress of the reaction was monitored through thin layer chromatography (TLC). After the completion of reaction, the reaction mixture was poured into the ice-cold water and stirred for a few minutes. The residue was filtered, washed with distilled water, purified by recrystallization with ethanol and filtered to afford desired products (Table 1) (65-94%). Characterization data for the synthesized products are as follows:

*N1-Phenyl-N3-(Thiophene-2-Carbonyl) Thiourea (**1**)*

Yellow solid, Yield 65%; mp. 155-156 °C; R_f 0.78 (Petroleum ether (PE)/EtOAc 1:2); H-NMR (400 MHz, DMSO-d6) δ (ppm): 12.46 (brs, 1H, N3H), 11.63 (brs,

Table 1. Synthetic derivatives of *N1*-(morpholin-4-yl ethyl)/phenyl/aralkyl *N3*-(thiophene-2-carbonyl)/benzoyl Thioureas

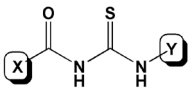

Comp. No.	X	Y	MW	Yield (%)
1	Thiophen-2-yl	Phenyl	262.02	65
2	Thiophen-2-yl	Thiophen-2-yl methyl	282.00	80
3	Thiophen-2-yl	4-Fluorophenyl methyl	294.03	94
4	Thiophen-2-yl	4-Chlorophenyl methyl	310.00	92
5	Thiophen-2-yl	Furan-2-yl methyl	266.02	82
6	Thiophen-2-yl	4-Methoxyphenyl methyl	306.05	91
7	4-Methoxyphenyl	Morpholin-4-yl ethyl	323.13	73
8	3-Chlorophenyl	Morpholin-4-yl ethyl	327.08	80
9	3,5-dinitrophenyl	Morpholin-4-yl ethyl	383.09	59
10	Thiophen-2-yl	Morpholin-4-yl ethyl	299.08	67
11	4-Fluorophenyl	Furan-2-yl methyl	278.05	88
12	4-Methylphenyl	Thiophen-2-yl methyl	290.05	87

1H, N1H), 8.40 (d, 1H, *J* = 3.6 Hz, CH Thiophene), 8.06 (d, 1H, *J* = 4.8 Hz, CH Thiophene), 7.68 (d, 2H, *J* = 7.6 Hz, CH Phenyl), 7.43 (t, 2H, *J* = 8.0 Hz, CH Phenyl), 7.26-7.30 (m, 2H, CH Phenyl and thiophene); ^{13}C-NMR (100 MHz, DMSO-d6) δ (ppm): 178.7, 162.0, 137.9, 136.6, 135.3, 132.7, 128.7, 128.6, 126.3, 124.7; IR (KBr) ν_{max} (cm^{-1}): 3440 (N3-H), 3283 (N1-H), 1661 (C = O), 1263 (C = S)

*N1-(Thiophen-2-yl Methyl)-N3-(Thiophene-2-Carbonyl) Thiourea (**2**)*

Pale yellow crystal, yield 80%; mp. 110-111 °C; R_f 0.62 (Petroleum ether (PE)/EtOAc 1:2); H-NMR (400 MHz, DMSO-d6) δ (ppm): 11.57 (s, 1H, N3H), 11.13 (brs, 1H, N1H), 8.41 (d, 1H, *J* = 4.0 Hz, CH Thiophene), 8.07 (d, 1H, *J* = 4.0 Hz, CH Thiophene), 7.50 (d, 1H, *J* = 3.6 Hz, CH Thiophene), 7.29 (t, 1H, *J* = 4.0 Hz, CH Thiophene), 7.19 (d, 1H, *J* = 4.0 Hz, CH Thiophene), 7.06 (t, 1H, *J* = 4.0 Hz, CH Thiophene), 5.09 (d, 2H, *J* = 5.6 Hz, CH_2); ^{13}C-NMR (100 MHz, DMSO-d6) δ (ppm): 179.8, 161.8, 139.4, 136.7, 135.1, 132.7, 128.8, 126.9, 126.6, 125.9, 42.9; IR (KBr) ν_{max} (cm^{-1}): 3409 (N3-H), 3147 (N1-H), 1653 (C = O), 1282 (C = S)

*N1-(4-Fuorophenyl Methyl)-N3-(Thiophene-2-Carbonyl) Thiourea (**3**)*

White crystal, Yield 94%; mp. 124-125 °C; R_f 0.80 (Petroleum ether (PE)/EtOAc 1:2); H-NMR (400 MHz, DMSO-d6) δ (ppm): 11.49 (s, 1H, N3H), 11.09 (brs, 1H, N1H), 8.35 (d,1H, *J* = 4.0 Hz, CH Thiophene), 8.02 (d, 1H, *J* = 4.0 Hz, CH Thiophene), 7.38-7.44 (m, 4H, CH Fluorobenzyl), 7.23 (t, 1H, *J* = 4.0 Hz, CH Thiophene), 4.85 (d, 2H, *J* = 6.0 Hz, CH_2); ^{13}C-NMR (100 MHz, DMSO-d6) δ (ppm): 180.2, 161.8, 136.8, 135.0, 133.6, 133.6, 132.4, 129.7, 129.7, 128.7, 47.3; IR (KBr) ν_{max} (cm^{-1}): 3305 (N3-H), 3182 (N1-H), 1654 (C = O), 1250 (C = S), 1163 (C-F)

*N1-(4-Chlorophenyl Methyl)-N3-(Thiophene-2-Carbonyl) Thiourea (**4**)*

White crystal, Yield 92%; mp. 127-128 °C; R_f 0.82 (Petroleum ether (PE)/EtOAc 1:2); H-NMR (400 MHz, DMSO-d6) δ (ppm): 11.50 (brs, 1H, N3H), 11.10 (brs, 1H, N1H), 8.35 (d, 1H, *J* = 4.0 Hz, CH Thiophene), 8.02 (d, 1H, *J* = 4.4 Hz, CH Thiophene), 7.44 (d, 2H, CH Chlorobenzyl), 7.41 (d, 2H, CH Chlorobenzyl), 7.23 (t, 1H, *J* = 4.0 Hz, CH Thiophene), 4.85 (d, 2H, *J* = 5.6 Hz, CH_2); ^{13}C-NMR (100 MHz, DMSO-d6) δ (ppm): 180.2, 161.8, 136.8, 136.5, 135.0, 132.4, 131.7, 129.4, 128.7, 128.3, 47.3; IR (KBr) ν_{max} (cm^{-1}): 3438 (N3-H), 3159 (N1-H), 1655 (C = O), 1262 (C = S), 731(C-Cl)

*N1-(Furan-2-yl Methyl)-N3-(Thiophene-2-Carbonyl) Thiourea (**5**)*

White Crystal, yield: 82%, mp: 100-101°C, R_f 0.86 (Petroleum ether (PE)/EtOAc 1:2); ^{1}H-NMR (400 MHz, DMSO-d6) δ (ppm): 11.50 (1H, s, N3H), 11.03 (brs, 1H, N1H), 8.30 (1H, d, *J* = 3.5 Hz, CH Thiophene), 8.00 (1H, d, *J* = 4 Hz, CH Thiophene), 7.60 (1H, d, CH Furan), 7.2 (1H, t, *J* = 4 Hz, CH Thiophene), 6.45 (1H, t, *J* = 2.5 Hz, CH Furan), 6.41 (1H, d, *J* = 2.8 Hz, CH Furan), 4.8 (2H, d, *J* = 6.5 Hz, CH_2); ^{13}C-NMR (100 MHz, DMSO-d6) δ (ppm): 180.1, 162.1, 149.9, 142.7, 136.6, 135.1, 132.5, 128.6, 110.5, 108.1, 41.4; FT-IR (KBr) ν_{max} (cm^{-1}): 3410 (N3-H), 3141 (N1-H Thiourea), 1651 (C = O), 1280 (C = S)

*N1-(4-Methoxyphenyl Methyl)-N3-(Thiophene-2-Carbonyl) Thiourea (**6**)*

White Crystal, yield 91%; mp. 97-98°C, R_f 0.79 (Petroleum ether (PE)/EtOAc 1:2); ^{1}H-NMR (400 MHz, DMSO-d6) δ (ppm): 11.52 (1H, s, N3H), 11.07 (brs, 1H, N1H), 8.40 (1H, d, *J* = 4 Hz, CH Thiophene), 8.0 (1H, d, *J* = 4.4 Hz, CH Thiophene), 7.2 (1H, t, *J* = 4 Hz, CH Thiophene), 7.3 (2H, d, *J* = 8.4 Hz, CH Phenyl), 6.9 (2H, d, *J* = 8.4 Hz, CH Phenyl), 4.8 (2H, d, *J* = 5.2 Hz, CH_2), 3.88 (3H, s, CH_3 methoxy); ^{13}C-NMR (100 MHz, DMSO-d6) δ (ppm): 179.8, 161.9, 158.6, 136.8, 135.0, 132.3, 129.1, 129.0, 128.7, 113.9, 55.1, 47.7; FT-IR (KBr) ν_{max} (cm^{-1}): 3400 (N3-H), 3200 (N1-H), 1659 (C = O), 1240 (C = S)

*General Procedure for the Synthesis of N1-(Morpholin-4-yl ethyl)-N3-(Thiophene-2-Carbonyl)/Benzoyl Thioureas (**7-10**)*

To a KSCN (1 mmol) in ethanol (15 mL), thiophene-2-carbonyl)/benzoyl chloride (1 mmol) was added. The reaction mixture was stirred for 10 min at room temperature and subsequently at 40 °C for 20 min. After appearance of the precipitate, amino ethyl morpholine (1 mmol) and triethylamine (3 drops) were added slowly into the solution and heated (40 °C) for 24 h. The progress of the reaction was monitored through TLC. After the completion of reaction, the reaction mixture was poured into the ice-cold water and stirred for a few minutes. The residue was filtered, washed with distilled water, purified by recrystallization with ethanol and filtered to afford

desired products (Table 1) (59-80%). Characterization data for the synthesized products are as follows:

*N1-(Morpholin-4-yl Ethyl)-N3-(4-Methoxy Benzoyl)-Thiourea (**7**)*

White Solid, yield: 73%; mp: 80-81°C; R_f 0.62 (Petroleum ether (PE)/EtOAc 1:2); H-NMR (400 MHz, DMSO-d6) δ (ppm(: 11.15 (s, 1H, N3H), 11.10 (brs, 1H, N1H), 7.96 1 (2H, d, *J* = 8.8 Hz, CH Phenyl), 7.04 (2H, d, *J* = 8.8 Hz, CH Phenyl), 3.84 (3H, s, OCH_3), 3.71 (2H, q, *J* = 6 Hz, CH_2), 3.60 (4H, t, *J* = 4.8 Hz, CH_2 Morpholine), 2.57 (2H, t, *J* = 6.4 Hz, CH_2), 2.43 (4H, brs, CH_2 Morpholine). ^{13}C-NMR (100 MHz, DMSO-d6) δ (ppm): 179.9, 167.2, 162.9, 130.0, 124.0, 113.6, 66.2, 55.5, 55.2, 52.9, 41.7; FT-IR (KBr) ν (cm^{-1}): 3239 (N3-H), 3152 (N1-H), 1664 (C = O), 1256 (C = S)

*N1-(Morpholin-4-yl Ethyl)-N3-(3-Chloro Benzoyl) Thiourea (**8**)*

Pink crystal, Yield 80%; mp. 120-121°C; R_f 0.77 (Petroleum ether (PE)/EtOAc 1:2) H-NMR (400 MHz , DMSO-d6) δ (ppm): 11.53 (1H, brs, N3H), 10.97 (brs, 1H, N1H), 7.98 (1H, s, CH Phenyl), 7.86 (1H, d, *J* = 8.0 Hz, CH Phenyl), 7.71 (1H, d, *J* = 8.0 Hz, CH Phenyl), 7.54 (1H, t, *J* = 8.0 Hz, CH Phenyl), 3.70 (2H, q, *J* = 6.0 Hz, CH_2), 3.60 (4H, t, *J* = 4.8 Hz, CH_2 Morpholine), 2.58 (2H, t, *J* = 6.0 Hz, CH_2), 2.43 (4H, brs, CH_2 Morpholine); ^{13}C-NMR 30 (100 MHz , DMSO-d6) δ (ppm): 179.6, 166.6, 134.3, 133, 132.5, 130.2, 128.3, 127.2, 66.2, 55.1, 52.9, 41.7; FT-IR (KBr) ν (cm^{-1}): 3167 (N1-H, N3-H, broad peak), 1664 (C = O), 1251 (C = S), 722 (C-Cl)

*N1-(Morpholin-4-yl Ethyl)-N3-(3,5-Dinitro Benzoyl)-Thiourea (**9**)*

Yellow crystal, Yield 59%; mp. 202-203 °C; R_f 0.83 (Petroleum ether (PE)/EtOAc 1:2); H-NMR (400 MHz , DMSO-d6) δ (ppm): 12.13 (1H, s, N3H), 10.90 (brs, 1H, N1H), 9.06 (2H, s, CH Phenyl), 9.02 (1H, s, CH Phenyl), 3.73 (2H, q, *J* = 6 Hz, CH_2), 3.61 (4H, t, *J* = 4.4, CH_2 Morpholine), 2.60 (2H, t, *J* = 6.0 Hz, CH_2), 2.45 (4H, brs, CH_2 Morpholine). ^{13}C-NMR (100 MHz, DMSO-d6) δ (ppm): 179.4, 164.2, 147.6, 135.4, 129.1, 121.1, 66.2, 55, 52.8, 41.8; FT-IR (KBr) ν (cm^{-1}): 3376 (N3-H), 3157 (N1-H), 1633 (C = O), 1275 (C = S)

*N1-(Morpholin-4-yl Ethyl)-N3-(Thiophene-2-Carbonyl)-Thiourea (**10**)*

Yellow solid, Yield 67%; mp. 142-143 °C; R_f 0.65 (Petroleum ether (PE)/EtOAc 1:2); H-NMR (400 MHz, DMSO-d6) δ (ppm): 11.38 (1H, s, N3H), 10.90 (brs, 1H, N1H), 8.35 (1H, d, *J* = 3.5 Hz, CH Thiophene) 8.00 (1H, d, *J* = 5.5 Hz, CH Thiophene), 7.23 (1H, t, *J* = 1.1 Hz, CH Thiophene) 3.70 (2H, q, *J* = 6.0 Hz, CH_2), 3.60 (4H, t, *J* = 5.0 Hz, CH_2 Morpholine), 2.57 (2H, t, *J* = 6.4 Hz, CH_2), 2.43 (4H, brs, CH_2 Morpholine). ^{13}C-NMR (100 MH, DMSO-d6) δ (ppm): 179.3, 161.8, 136.8, 134.8, 132.3, 128.0, 66.2, 55.2, 52.9, 41.8; FT-IR (KBr) ν (cm^{-1}): 3248 (N3-H), 3140 (N1-H), 1642 (C = O), 1268 (C = S)

*General Procedure for the Synthesis of N1-Phenyl/Aralkyl-N3-(Thiophene-2-Carbonyl) Thioureas (**11** and **12**)*

To a KSCN (1 mmol) in acetonitrile (15 mL), benzoyl chloride (1 mmol) was added. The reaction mixture was stirred for 1 h at room temperature. After appearance of the precipitate, corresponding amine (1 mmol) and triethylamine (3 drops) were added slowly into the solution and heated (40 °C) for 24 h. The progress of the reaction was monitored through TLC. After the completion of reaction, the reaction mixture was poured into the ice-cold water and stirred for a few minutes. The residue was filtered, washed with distilled water, purified by recrystallization with ethanol and filtered to afford desired products (Table 1) (87%-90%). Characterization data for the synthesized products are as follows:

*N1-(Furan-2-yl Methyl)-N3-(4-Fluorophenyl)-Thiourea (**11**)*

Pale yellow solid, Yield 88%; mp. 127-129°C, R_f 0.77 (Petroleum ether (PE)/EtOAc 1:2); ^{1}H-NMR (400 MHz, DMSO-d6) δ (ppm): 11.54 (1H, s, N3H), 11.12 (s, 1H, N1H), 8.03 (2H, d, *J* = 5.6 Hz, CH phenyl), 7.99 (2H, d, *J* = 5.2 Hz, CH phenyl), 7.66 (1H, brs, CH Furan), 7.34 (1H, t, *J* = 9.2 Hz, CH Furan), 6.44 (1H, d, *J* = 2 Hz, CH Furan), 4.87 (2H, d, *J* = 5.2 Hz, CH_2); ^{13}C-NMR (100 MHz, DMSO-d6) δ (ppm): 180.1, 169.4, 166.0, 148.9, 142.3, 129.8, 129.2, 115.5, 110.6, 106.6, 41.5; FT-IR (KBr) ν_{max} (cm^{-1}): 3416 (N3-H), 3155 (N1-H), 1666 (C = O), 1266 (C = S), 1159 (C-F)

*N1-(Thiophen-2-yl Methyl)-N3-(4-Methylphenyl)-Thiourea (**12**)*

Pale yellow crystal, Yield 87%; mp. 110-111 °C, R_f 0.61 (Petroleum ether (PE)/EtOAc 1:2); ^{1}H-NMR (400 MHz, DMSO-d6) δ (ppm): 11.38 (1H, s, N3H), 11.23 (brs, 1H, N1H), 7.85 (2H, d, *J* = 8.4 Hz, CH Phenyl), 7.45 (2H, d, *J* = 5.2 Hz, CH Phenyl), 7.31 (1H, d, *J* = 8 Hz, CH Thiophene), 7.15 (1H, d, *J* = 2.4 Hz, CH Thiophene), 7.01 (1H, t, *J* = 4.8 Hz, CH Thiophene), 5.05 (2H, d, *J* = 5.6 Hz, CH_2), 2.38 (3H, s, CH_3); ^{13}C-NMR (100 MHz, DMSO-d6) δ (ppm): 179.6, 169.0, 143.7, 139.5, 131.0, 128.8, 127.1, 126.9, 126.7, 125.8, 42.9, 24.2; FT-IR (KBr) ν_{max} (cm^{-1}): 3152 (N1-H, N3-H, broad peak), 1674 (C = O), 1257 (C = S)

Biological Assessment

Reagents and Chemicals

Fetal bovine serum (FBS), Roswell Park Memorial Institute 1640 (RPMI 1640), trypsin, and phosphate-buffered saline (PBS) were all purchased from Biosera (Ringmer, UK). 3-(4,5-dimethylthiazol-2-yl)-2,5-diphenyltetrazolium bromide (MTT) (3-(4,5-dimethylthiazol-2-yl)-2,5-diphenyltetrazolium bromide) was acquired from Sigma (Saint Louis, MO, USA), and penicillin/streptomycin was purchased from Invitrogen (San Diego, CA, USA). *Cis*-platin and dimethyl sulphoxide (DMSO) were obtained from EBEWE Pharma (Unterach, Austria) and Merck company (Darmstadt, Germany), respectively.

Evaluation of Cytotoxicity by MTT Assay

Cell viability following exposure to the synthetic compounds was estimated via MTT reduction assay.[32] AGS cells were plated in 96-well microplates at a density of 1×10^4 cells per well in RPMI 1640 medium supplemented with 10% FBS and 1% pen/strep for 24 h and then, the culture medium was changed to a medium containing the desired volume of the synthetic compounds (which were firstly dissolved in DMSO and then diluted in medium). After 24 h of culture, the medium was removed and MTT solution was added to each well at a final concentration of 0.5 mg/mL, and the plates were incubated for further 4 h at 37 °C in a dark condition. Then, the resulted formazan crystals were solubilized in 200 µL DMSO and optical density was measured at 570 nm with background correction at 570 nm using a Bio-Rad microplate reader (Model 680, USA). Control wells contained no drugs and blank wells contained only growth medium for background correction. The percentage of cell viability compared to the control wells was calculated for each concentration of the compounds and IC_{50} values were calculated with Sigma Plot version 12.5. In all groups, the absorbance of wells containing no cells (Blank) was subtracted from the sample well absorbance.

Wound Healing Assay

To evaluate the cell migration property following treatment, AGS cells (6×10^4) were seeded onto 24-well plates to grow in a monolayer (48 h). Then a sterile 100-200 µL pipette tip was held vertically to scratch a cross in each well. The detached cells were removed by washing with 500 µL PBS. Then 6.25 and 12.5 µg/mL concentrations of the compounds were prepared by dilution with medium. In the next step, the medium of the wells was removed and the first column of the plate was treated as control and the next columns were treated with intended concentrations. After 24, 48 and 72 hours, photos with Olympus CKX41 inverted microscope were taken using cellSens software, standard 1.14 equipped with DP27 camera.[33]

In Silico Studies

Drug-Likeness

Overall drug-likeness scores and Number of H-bond donors/acceptors were calculated by MolSoft tool (https://molsoft.com/mprop/). Pharmacokinetics properties were estimated by SwissADME online server.[34,35]

Molecular Docking

Lamarckian genetic algorithm (LGA) of AutoDock4.2 software was used to run ligand flexible docking simulations on thiourea compounds.[36,37] All the preparation procedure for ligand, receptor and docking parameters were performed according to the previous protocols.[29] Post-docking analysis of ligand-protein interactions were estimated and visualized by protein-ligand interaction profiler (PLIP) fully automated server.[38,39] Crystallographic *Homo sapiens* 3D structure of RhoA in complex to its inhibitor (PDB code 5JHH) was retrieved from Brookhaven protein data bank (PDB; www.rcsb.org) with the structural resolution of 2.30 Å.[40] It should be notified that the retrieved holo structure contained a quinoline based ligand (Designated as RAO) (Supplementary file 1).

Molecular Dynamics

All-atom MD simulations were performed for 60 ns with GROningen MAchine for chemical simulations (GROMACS 5.1.1) software.[41] Topology files and other force field parameters for thiourea derivatives were generated by ATB (Automated topology builder) server.[42] Water molecules were considered by a simple point charge (SPC216) model. Overall charge neutrality of the complex system was acquired through insertion of 7 Na^+ ions. GROMOS96 54a7 force field of the GROMACS was used to determine chemical interactions.[43] Energy minimization of the protein-ligand complex was done by steepest descent followed by conjugate gradient algorithms via stopping the minimization when the maximum force achieved ≤ 1000 kJ/mol/nm. Subsequent to energy minimization process, position restraint step was performed in association with NVT (Number of particles, volume, temperature) and NPT (Number of particles, volume, temperature) ensembles. An NVT ensemble was adopted at constant temperature of 300 K with a coupling constant of 0.1 ps and time duration of 500 ps. NPT ensemble was performed under a constant pressure of 1 bar and a coupling constant of 5.0 for 1000 ps. The pressure was held constant with the Parrinello-Rahman barostat.[44] The lincs algorithm for covalent bond constraints was applied.[45] The particle-mesh Ewald (PME) and cut-off methods were used to determine the long-range electrostatic and van der Waals interactions, respectively.[46] Protein surface areas were obtained by rolling a 1.4 Å sphere on the molecular surface.[47]

Results and Discussion

Chemistry

Chemical structures of synthesized *N3*-(thiophene-2-carbonyl)/benzoyl-*N1*-(morpholin-4-ethyl)/phenyl/aralkyl thiourea derivatives were confirmed by FT-IR, H-NMR, and ^{13}C-NMR methods. Melting points and TLC retention indices (R_f) in different ratios of petroleum ether and ethyl acetate were reported for each compound. Synthetic routs to compounds **1**-**12** is depicted in Scheme 1. Form the mechanistic point of view, the initial synthetic step comprised a nucleophilic attack of potassium thiocyanate nitrogen to acid halide and leaving of chloride ion. Subsequent capture of thiocarbonyl intermediate with corresponding amines afforded carbonyl thiourea products (59-94%) (Scheme 1).

On the basis of H-NMR data, hydrogen atoms attached to the N3 of carbonyl thiourea derivative exhibited the most down field peaks (δ 11.15-12.46 ppm) due to their position between carbonyl and thiocarbonyl moieties as

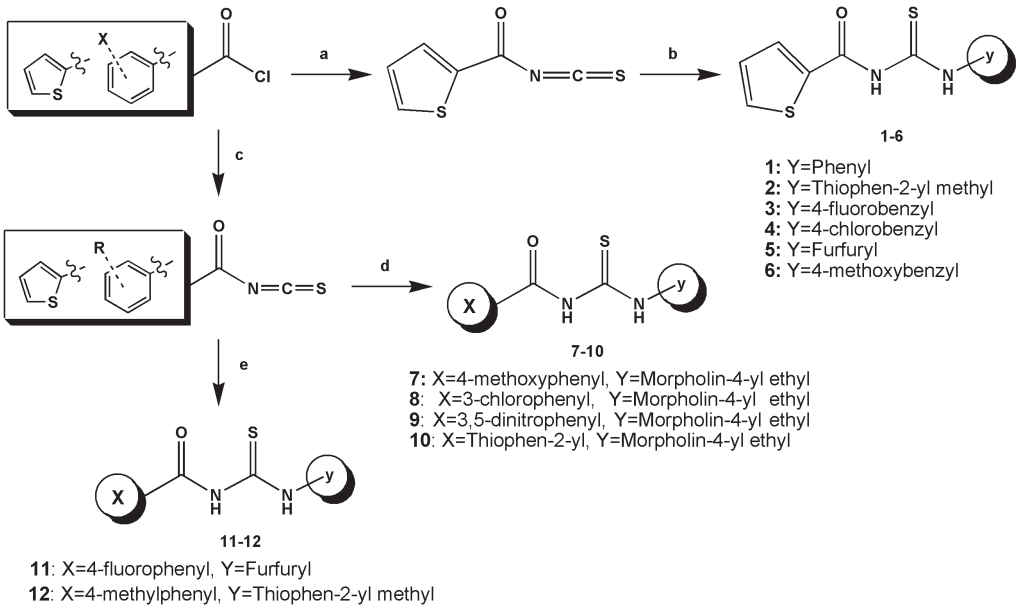

Scheme 1. Synthetic route of N1-(morpholin-4-ethyl)/phenyl/aralkyl-N3-(thiophene-2-carbonyl)/benzoyl thioureas (1-12); a) KSCN, Acetonitrile, 1 h (RT); b) R/ArNH2, triethylamine, 24 h, 40 °C; c) KSCN, Acetonitrile, 1 h (RT); d) Amino ethyl morpholine, triethylamine, 24 h, 40 °C; e) RNH2, triethylamine, 24 h, 40 °C

two electron withdrawing groups (EWGs). As reported for related compounds,[29,48] with regard to N3H, hydrogens of N1 atom were a bit more shielded and hence appeared at 10.90 to 11.63 ppm since they were not located near the carbonyl group. All the hydrogen atoms attached to the N1 atoms appeared as the broad singlet peak. For compounds **1**-**6** including thiophene ring attached to the carbonyl group, the hydrogens which are attached to the carbon atom adjacent to sulfur appeared at 8.30-8.40 ppm due to the de-shielding effect of sulfur atom. Compounds **2** and **12** had thiophene ring which was attached to the thiocarbonyl ring through alkyl linker and appeared at more de-shielded chemical shifts (7.29 and 7.31 ppm) due to the lack of EWG on the thiophene ring with regard to the same hydrogen in thiophene carbonyl moiety. Thiophene rings of compounds **2** and **12** could be comparable to the furan rings of compounds **5** and **11**, respectively. In compounds 5 and 11, similar hydrogen atoms which were closest to the heteroatom appeared at more de-shielded chemical shifts (7.60 and 7.66 ppm) due to the more electronegativity of oxygen atom than sulfur. In all H-NMR spectra, peaks appeared around 2.50 and 3.35 ppm belong to the solvent. The most de-shielded phenyl hydrogen atoms belonged to the compound **9** (9.02 and 9.06 ppm) with two strong electronegative nitro substituents.[49] Compounds **7**-**10** included ethyl morpholine moiety and a peak that appeared as a quartet (3.70-3.73 ppm) belonged to the methylene hydrogens that were attached to the N1H group. Within the morpholine ring, hydrogens located near oxygen atom exhibited higher chemical shifts (3.60 ppm) with regard to the similar hydrogens near less electronegative nitrogen atom (2.43 ppm).[50,51]

In the FT-IR spectrum, stretching vibrations of N3-H bonds led to a broad and intense peak with ν_{max} of 3239 to 3440 cm^{-1} in compounds **1**-**12**. N1-H bond showed vibrational peaks in the range of 3140-3283 cm^{-1} in various derivatives.[29] Carbonyl vibrational peak appeared in the range of 1633-1674 cm^{-1} for different derivatives which are located at lower wavenumber values due to the resonance between carbonyl bond and aromatic ring. Thiocarbonyl vibrational bonds appeared in the range of 1240-1282 cm^{-1}.[29,52] The vibrational peak at 722 cm^{-1} at compound **8** was assigned to the C-Cl bond which is in excellent agreement with previous reports on similar carbonyl thiourea derivatives.[53] In compounds **3** and **11**, the vibrational peak at 1163 and 1159 cm^{-1} were assigned to the C-F bond stretching, respectively. Within a ^{13}C-NMR spectra, the number of existed bands were equal to the number of types of carbon atom in synthetic derivatives. The most down-field bands attributed to the carbon atom of thiocarbonyl group (179.3-180.2 ppm) followed by carbon in the case of atoms of carbonyl moieties (161.8-169.4 ppm).[29,52]

Drug-Likeness

Overall drug-likeness and a few pharmacokinetics properties of the synthesized thiourea derivatives were estimated by MolSoft and SwissADME servers (Table 2) (Supplementary file 2). It has been postulated that compounds possessing zero or negative drug-likeness scores do not seem to be a drug-like structures, and values greater than zero could be regarded as drug-like compounds.[54] Average drug-likeness score of the synthetic derivatives (**1**-**12**) was found to be 0.09. Unlike Compounds **3**, **4** and **7**-**11** that could be categorized in the region of Food and Drug Administration (FDA) approved drugs, derivatives **1**, **2**, **5**, **6** and **12** showed a bit violation from the drug-like region.

SwissADME driven data indicated that candidate

molecules had high gastrointestinal (GI) absorption and the only exception with low GI absorption was compound **9** bearing two hydrophilic nitro groups. Moreover, with the exception of derivatives **7** and **9**, all the compounds seemed not to be a P-glycoprotein (P-gp) substrate and hence showed probably lower risk of producing drug-resistance via efflux pump. None of the thiourea compounds showed potential blood brain barrier (BBB) penetration implying that the intended derivatives would probably not cause serious side effects to central nervous system (CNS).

Biological Assessment

Cytotoxicity Assessment

Cytotoxic effects of compounds **1**-**12** against AGS cell lines are summarized in Table 3. As indicated by the results, within low concentrations, cytotoxic effects of thiourea derivatives are not significantly different with respect to the solvent (DMSO 2%). Since the cytotoxicity of the synthetic derivatives were not significant within medium to low doses, it was preferred to report the percentages of viability (or death) and compare the results of cytotoxicity within definite concentrations. Cytotoxic effects were superior after applying 50 µg/mL dose of compound **4** (AGS cell viability 40.57%). This compound was demonstrated to be the most cytotoxic derivative among synthesized derivatives. Higher cytotoxic effect of compound **4** was more apparent at 100 µg/mL (AGS cell viability 9.44%) and 200 µg/mL (AGS cell viability 3.15%). Other thiourea derivatives exhibited AGS cell viabilities of 57.35-86.50% and 8.97-65.21% at 100 and 200 µg/mL doses, respectively. Following compound **4**, compound **11** showed higher cytotoxic effects at 50 and 100 µg/mL doses and led to the 60.65% cell death at 200 µg/mL dose. Dose dependent diagrams for compounds **4** and **11** in terms of cell survival (viability) are depicted in Figure 1.

Table 2. Overall drug-likeness and a few pharmacokinetics of *N1*-(morpholin-4-yl ethyl)/phenyl/aralkyl-*N3*-(thiophene-2-carbonyl)/benzoyl thioureas

Comp. No.	HBD	HBA	Drug-likeness score	TPSA[a] (Å^2)	Consensus logP	GI absorption	BBB permeant	P-gp substrate
1	2	3	-0.80	101.46	2.81	High	No	No
2	2	4	-0.46	129.70	2.83	High	No	No
3	2	3	0.00	101.46	3.16	High	No	No
4	2	3	0.22	101.46	3.38	High	No	No
5	2	4	-0.51	114.60	2.24	High	No	No
6	2	4	-0.26	110.69	2.88	High	No	No
7	2	5	1.07	94.92	1.46	High	No	Yes
8	2	4	0.88	85.69	1.96	High	No	No
9	2	8	0.35	177.33	-0.09	Low	No	Yes
10	2	5	0.67	113.93	1.51	High	No	No
11	2	3	0.02	86.36	2.41	High	No	No
12	2	3	-0.06	101.46	3.15	High	No	No

[a] TPSA stands for topological polar surface area which is the sum of surface areas for nitrogen and oxygen atoms and their attached hydrogens.

Table 3. Percentage of AGS cell viability upon treatment with different concentrations of *N1*-(morpholin-4-yl ethyl)/phenyl/aralkyl-*N3*-(thiophene-2-carbonyl)/benzoyl thioureas

Comp. No	Viability% [a] ± SEM in different doses (µg/mL) of compounds					
	6.25	12.5	25	50	100	200
1	98.88 ± 2.00	97.30 ± 1.74	96.53 ± 1.69	93.29 ± 1.66	82.12 ± 2.45	46.30 ± 4.51
2	92.02 ± 3.09	87.03 ± 7.40	88.49 ± 8.34	77.19 ± 7.52	61.38 ± 2.05	35.61 ± 13.53
3	101.10 ± 4.46	98.33 ± 1.92	91.10 ± 6.22	85.10 ± 2.82	84.84 ± 2.32	13.28 ± 1.76
4	99.74 ± 16.44	95.12 ± 17.92	85.23 ± 15.35	40.57 ± 6.02	9.44 ± 2.08	3.15 ± 1.12
5	113.98 ± 11.26	107.83 ± 1.62	104.59 ± 10.65	101.20 ± 12.14	82.49 ± 15.59	65.21 ± 6.59
6	81.87 ± 0.61	78.63 ± 0.83	78.13 ± 0.68	74.77 ± 1.45	74.45 ± 1.75	65.17 ± 1.32
7	100.16 ± 12.05	97.59 ± 13.32	96.14 ± 11.57	95.65 ± 12.21	86.50 ± 15.42	60.93 ± 18.80
8	96.78 ± 1.28	96.78 ± 1.22	96.09 ± 3.61	90.34 ± 1.61	77.93 ± 2.39	8.97 ± 7.47
9	96.95 ± 9.25	95.05 ± 7.20	93.71 ± 5.16	86.95 ± 5.73	65.14 ± 2.15	15.96 ± 10.02
10	102.91 ± 0.85	101.83 ± 1.74	100.46 ± 1.06	95.57 ± 4.02	82.72 ± 5.71	54.74 ± 3.79
11	92.64 ± 8.18	80.74 ± 8.73	75.72 ± 7.85	69.57 ± 7.00	57.35 ± 6.55	39.35 ± 6.00
12	81.00 ± 9.33	78.36 ± 8.60	74.88 ± 10.3	71.49 ± 9.18	66.11 ± 9.75	54.40 ± 10.72
Cis-Platin[b]	68.44 ± 7.36	49.09 ± 6.77	26.31 ± 4.10	17.25 ± 2.98	7.11 ± 1.25	0.20 ± 0.02

[a] Data are presented as mean ± SEM (n = 3), for cis-platin the IC_{50} (µg/mL) ± SEM is reported. [b] The IC_{50} of cis-platin was acquired as 11.47 ± 1.35 µg/mL.

In the case of compound **4**, cell cytotoxicity effect emerged as a curvature with steeper slope following 25 µg/mL dose. Derivative **9** exhibited similar trend but the relevant curvature showed steeper slope in comparison with compound **4** and emerged after 50 µg/mL. It seemed that the introduction of morpholin-2-yl ethyl moiety significantly decreased the cytotoxic effects of thiourea derivatives with regard to phenyl and benzyl substituents. Although not being statistically significant, results indicated relatively enhanced cytotoxicity of compounds **8** and **9** at higher doses among the morpholine bearing structures (Table 3). This observation could be further clear when the cytotoxic effect of compound **7** was compared with the effects of its close analogues *N*1-(4-fluorophenyl methyl)-*N*3-(4-methoxybenzoyl) thiourea (IC_{50} 9.39 µg/mL), *N*1-(4-chloroophenyl methyl)-*N*3-(4-methoxybenzoyl) thiourea (IC_{50} 14.57 µg/mL), *N*1-(4-methoxyphenyl methyl)-*N*3-(4-methoxybenzoyl) thiourea (IC_{50} 3.67 µg/mL) and *N*1-(thiophen-2-yl methyl)-*N*3-(4-methoxybenzoyl) thiourea (IC_{50} 21.75 µg/mL) in our previous work.[29] Another supporting example could be denoted through comparing the cytotoxicity of compound **8** and *N*1-(thiophen-2-yl methyl)-*N*3-(3-chlorobenzoyl) thiourea derivative (IC_{50} 20.27 µg/mL) (29). Moreover; when thiophen-2-yl methyl was substituted at thiourea *N*1 instead of benzoyl moiety (Compound **2**), potent cytotoxic effect of *N*1-(thiophen-2-yl methyl)-*N*3-(3-chlorobenzoyl) thiourea could not be re-achieved.

Similar comparisons between compound **3** and its close structural analogues, *N*1-(4-chlorophenyl methyl)-*N*3-(4-fluorobenzoyl) thiourea and *N*1-(4-chlorophenyl methyl)-*N*3-(4-methoxybenzoyl) thiourea or compound **4** and its close structural analogues, *N*1-(4-fluorophenyl methyl)-*N*3-(4-methoxybenzoyl) thiourea and *N*1-(4-fluorophenyl methyl)-*N*3-cyclopropanoyl thiourea,[29] revealed that the replacement of benzoyl substituents with thiophen-2-carbonyl moiety at N3 position of thiourea led to the significant decrease of cytotoxic effects.

Cell Migration Inhibitory Effect by Wound Healing Assay

As depicted in Figure 2, AGS cells transited from the epithelial state to the mesenchymal phenotype with distinct processes and fusiform morphology. The acquired morphology enables cancer cells to migrate from the primary location and thus wound-healing effect can be observed. Results of the in vitro wound-healing assay at 6.25 and 12.5 µg/mL doses of compounds **1-12** at 24, 48 and 72 h with regard to the untreated cells (control group) are depicted in Figures 3-5. It was also assured that cell migrations in untreated and DMSO-treated media were comparable to each other and significant wound coverage occurred after 24 h culture (Supplementary file 3). C*is*-platin was used as the positive control in the assessment and inhibited the wound-healing of AGS cells within IC_{50} value (11.49 µg/mL) (Figure 6).

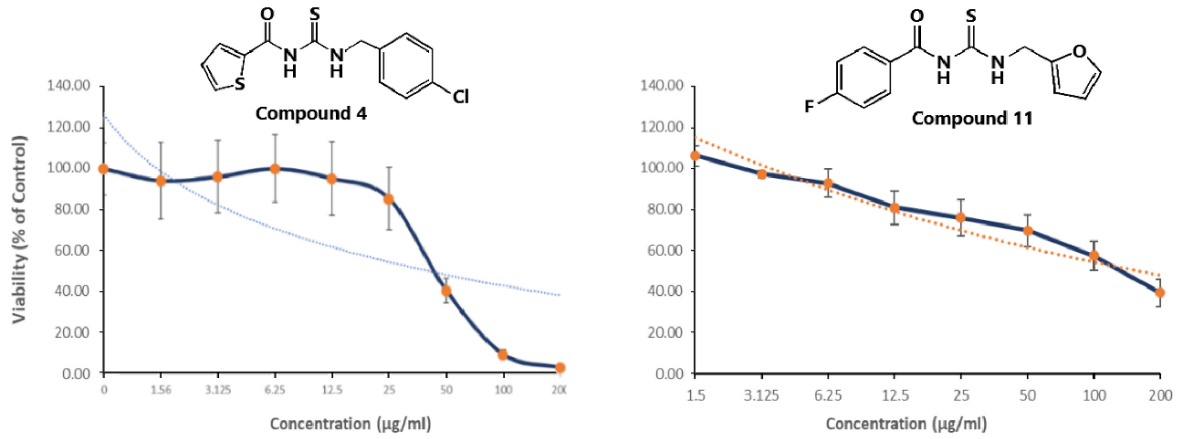

Figure 1. Percentage of AGS cell viabilities in different doses of carbonyl thiourea derivatives (4 & 11)

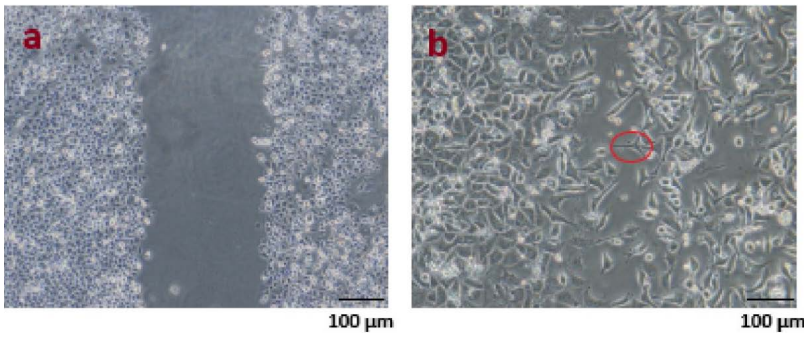

Figure 2. Photomicrograph of AGS cells after cross scratching and b) Migrating AGS cells which underwent EMT and appeared mesenchymal phenotype with short processes and fusiform morphology after 24 h treatment with compounds to heat the wound

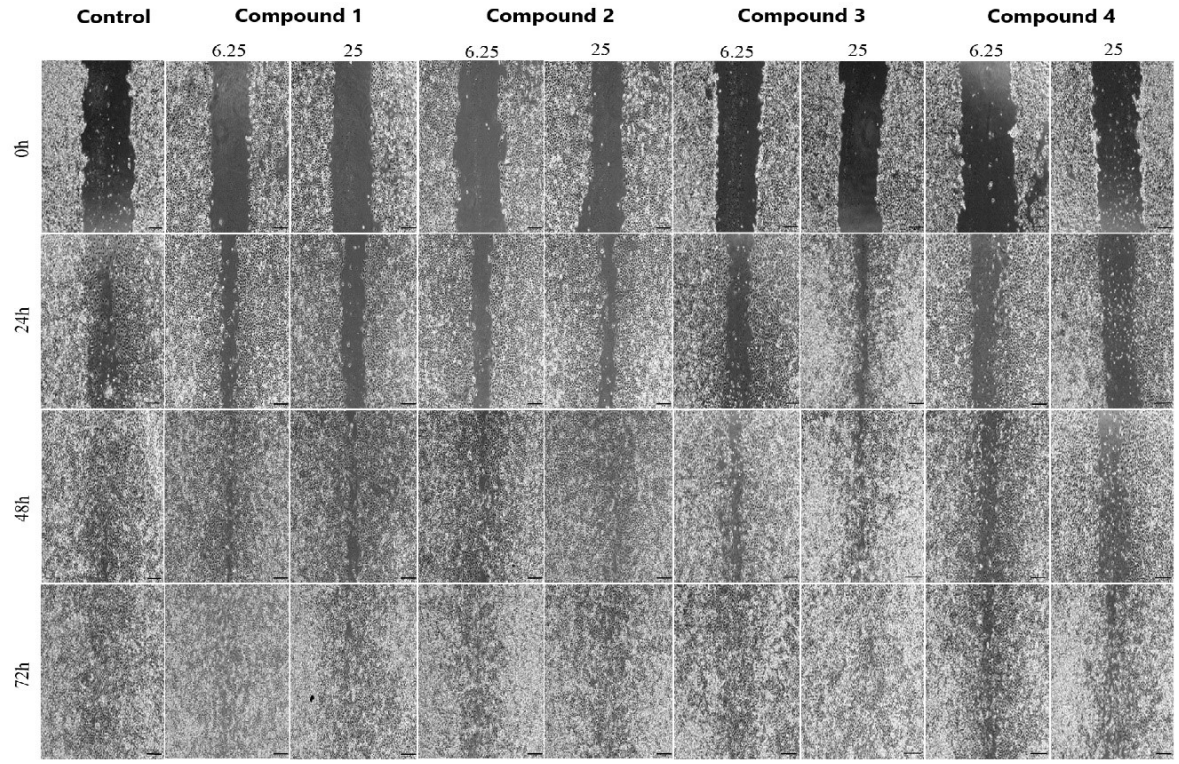

Figure 3. Photomicrographs of migrated AGS cells in the presence of DMSO (control) and 6.25 and 12.5 µg/mL doses of compounds 1-4 after 24, 48 and 72 h treatment

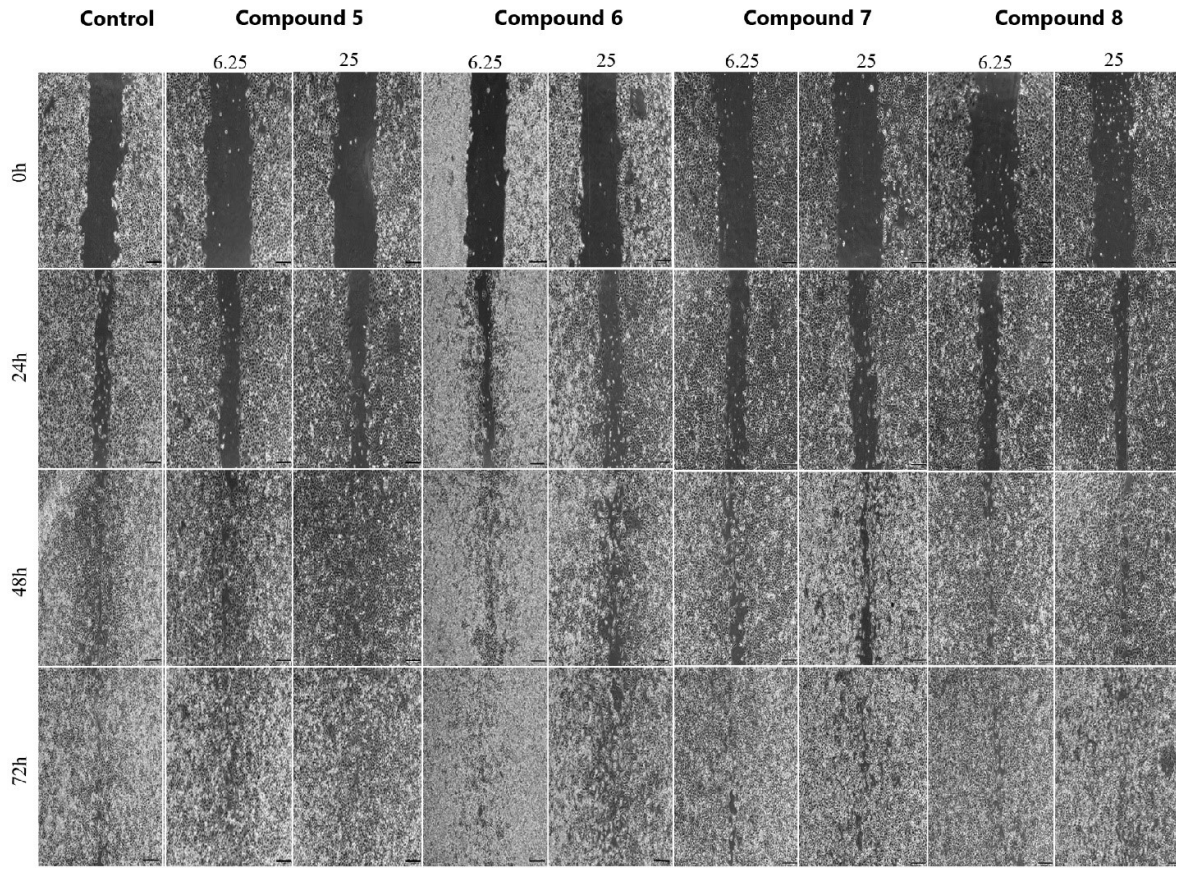

Figure 4. Photomicrographs of migrated AGS cells in the presence of DMSO (control) and 6.25 and 12.5 µg/mL doses of compounds 5-8 after 24, 48 and 72 h treatment

All of the compounds could relatively inhibit wound-healing process after 24 h, although some derivatives were observed to be better migratory inhibitors. Compound **4** and to some extent compound **12** exhibited superior wound-healing inhibitions with regard to the control group at the intended doses. The inhibition effect of

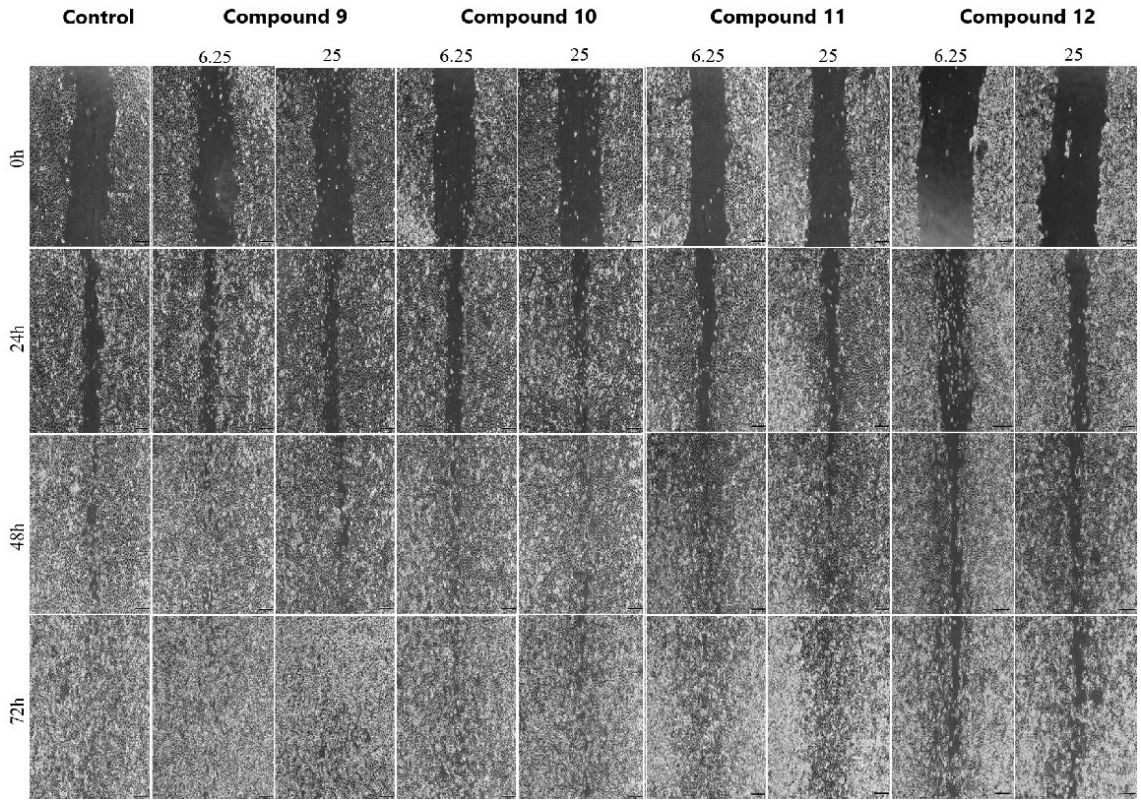

Figure 5. Photomicrographs of migrated AGS cells in the presence of DMSO (control) and 6.25 and 12.5 µg/mL doses of compounds 9-12 after 24, 48 and 72 h treatment

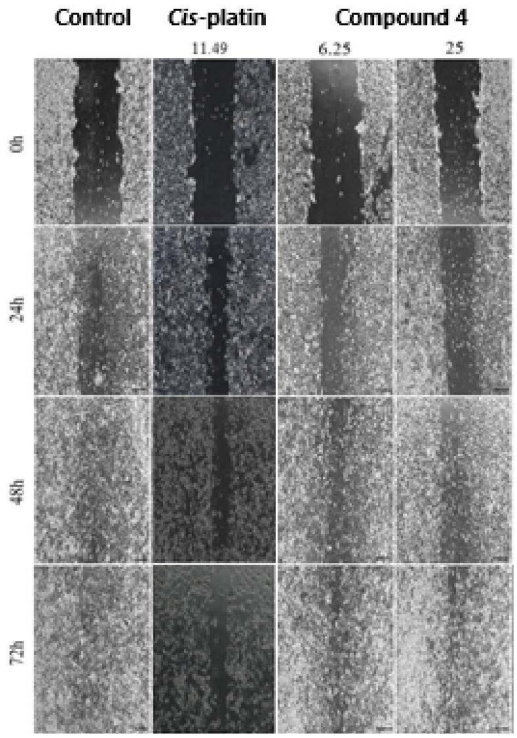

Figure 6. Photomicrographs of migrated AGS cells in the presence of IC50 dose of cis-platin and 6.25 and 12.5 µg/mL doses of compounds 4 after 24, 48 and 72 h treatment

derivative **4** was less noticeable following 48 h treatment but still better than the other thiourea compounds. Unlike compound **4**, other derivatives led to the complete wound-healing effect after 72 h treatment.

Our results specified that compound **4** could be further evaluated and developed as potential anti-metastatic agent in invasive AGS cancer cells. The structures with the characteristics of compounds **4** are appropriate candidates since they may inhibit tumor migration via more metastatic mechanisms, without any interfering cytotoxic effects.[19] Although highest cytotoxic effect against AGS cancer cells was indicated by compound **4**, the MTT assay indicated that compounds **4** and **12** could not be demonstrated as potent cytotoxic agent against AGS cells in concentrations below 50 µg/mL. Non/weak-cytotoxic cell migration inhibitors have advantage over the potent cytostatic agents due to their probable more selective anti-metastatic effects. To be noted, *N*1-substutued phenyl-*N*3-benzoyl thiourea derivatives have been previously demonstrated to inhibit cancer cell migration without any significant cellular toxicity effects.[24]

Molecular Docking

We were prompted to predict the probable binding pose/affinity of carbonyl thiourea derivatives in the binding site of RhoA. RhoA is a validated oncogenic target in cell adhesion, migration and metastasis of gastric cancer. In a biological context, RhoA is an intracellular GTPase with determinant role in progression of gastric cancer cells with higher expression in comparison to other adjacent tissues.[30,31] Moreover, RhoA is involved in EMT process and actin remodeling which supports its significance in targeting cell migration and metastatic gastric cancer.[31] A few studies have also revealed that the focal adhesion

kinase-RhoA (FAK–RhoA) pathway may influence cancer cell motility.[55,56]

Validation of docking method was evaluated through extraction of a co-crystallographic ligand and it's re-docking into the designated protein binding site. Root mean square deviation (RMSD) between re-docked and primary co-crystallized ligand conformation is the criteria of validation which needs to be ≤ 2 Å. On the basis of re-docking results, appropriate predictability levels (1.64 Å) could be achieved after 50 independent genetic algorithm (GA) runs, and 2.5×10^7 maximum number of energy evaluations (For more information, refer to Supplementary file 1).

Molecular docking procedure was applied to obtain the desired binding conformations and their respective affinities to the target protein. With regard to the obtained docking scores (Table 4), none of the carbonyl thioureas had more affinity than the corresponding co-crystallographic ligands. This result might be expected due to the induced fit phenomenon between RhoA structure and relevant bound ligand. Compound **9** was the top-ranked derivative in binding to RhoA GTPase site (ΔG_b -6.75 kcal/mol) but on the basis of cell migration assessments and also low energy differences, compound **4** was selected for our further structural analysis through MD simulations. Furthermore, top-scored cluster of compound 4 was supported by higher conformational population (40%). It should be noted that docking-based binding conformation of compound **4** is going to be represented and compared with the MD-driven interaction model in next section. With regard to the mechanistic correlation of RhoA functionality to gastric cancer cell migration and metastasis, binding mechanism of candidate inhibitors may assist in deriving applicable structure binding relationships and devise new and more potent RhoA inhibitors.[31]

Table 4. AutoDock 4.2 estimated binding energies between *N1*-(morpholin-4-yl ethyl)/phenyl/aralkyl-*N3*-(thiophene-2-carbonyl)/benzoyl thiourea derivatives and human RhoA GTP-binding site (PDB code: 5JHH)

Comp. No.	Mean ΔG_b (kcal/mol)	Highest ΔG_b in cluster (kcal/mol)
1	-5.01	-5.31
2	-4.94	-5.46
3	-5.02	-5.30
4	-5.42	-5.96
5	-4.88	-5.51
6	-5.39	-5.88
7	-5.28	-5.59
8	-5.36	-5.78
9	-5.75	-6.31
10	-4.68	-5.09
11	-5.16	-5.43
12	-5.06	-5.32
Co-crystallographic Inhibitor	-7.37	-7.90

MD Simulations of Promising Candidate

Compound **4** included *para*-chlorophenyl methyl and thiophene-2-carbonyl substituents at thiourea N1 and N3 sites and was found as the top-scored inhibitor of the AGS cell migration. Following docking analysis, stable binding mode of compound **4** was elucidated with respect to the dynamic features of RhoA structure. For this purpose, MD simulations were carried out on RhoA-compound **4** complex throughout 60 ns time scale. Conformations from each MD trajectory were used to evaluate root mean square deviation (RMSD), root mean square fluctuation (RMSF), radius of gyration (Rg), intramolecular/intramolecular H-bonds and solvent accessible surface area (SASA) of the RhoA structure upon binding to compound **4**. For comparison purposes, the apo form of the RhoA structure was also subjected to MD simulations.

Analysis of RhoA Structure

As depicted in Figure 7a, RhoA reached to the more stable phase upon binding to compound **4** and after about 25 ns. The apo state achieved a more stable phase a bit earlier. The observed RMSD patterns indicated that RhoA structures (Complex and apo) converged to the equilibrium state although the apo conformation was associated with lower RMSDs (Average value 0.22 ± 0.02 nm) with regard to the complex (Average value 0.28 ± 0.03 nm). The coefficient variation (CV) of RMSD for RhoA structures were found to be 11.55 and 11.44%, correspondingly. It was revealed that RMSF variation patterns of RhoA Cα atoms conformed to each other in complex and apo conformations (Figure 7b). The average RMSF values for RhoA backbone Cα atoms were estimated to be 0.15 ± 0.01 and 0.14 ± 0.01 nm for complex and apo state, respectively. Despite similar distribution patterns, most of the residues showed higher fluctuations upon presence of compound **4** with regard to their apo state. Val33 (Complex 0.48 nm, apo 0.34 nm) and Gln63 (Complex 0.36 nm, apo 0.21 nm) and Val24 (Complex 0.25 nm, apo 0.14 nm) were the most fluctuated residues (> 0.1 nm) in the RhoA structure. These highly flexible residues were not found in the binding site, but might be essential for retaining the ligand through conferring structural flexibility. Val33 and Gln63 resided in switch I and II of the RhoA structure (Figure 7b), respectively, and on the basis of previous structural investigations, switch regions were highly dynamic.[57] Switch regions of RhoA are important sites for nucleotide binding and their conformational changes is correlated well to GDP/GTP exchange.[58] It has been revealed that the dynamic equilibrium of the Switch I region provides interactions to guanine nucleotide exchange factors (GEFs) and GTPases activating proteins (GAPs).[59] Interestingly, there were some residues (33.7%) that showed lower flexibilities upon presence of compound **4**. Asp13 (ΔRMSF -0.08 nm), Gly14 (ΔRMSF -0.09 nm) and Gly50 (ΔRMSF -0.07 nm), Arg70 (ΔRMSF -0.06 nm) and Pro71 (ΔRMSF -0.05 nm) were the amino acid residues that showed noticeable RMSF decrements upon

presence of compound **4** (< 0.05 nm).

The compactness of RhoA structure in complex system was checked by estimation of Rg during MD simulations (Figure 7c). Rg variation patterns were comparable for both complex and apo states and it was found that RhoA backbone could preserve its appropriate folding after binding to compound **4**. Average Rg values were found to be 1.59 ± 0.01 and 1.58 ± 0.01 nm for the complex and apo state with very low variations (CV 0.73 & 0.60%), respectively. Structural stability was also evaluated through persistence of RhoA intramolecular H-bonds during MD time (Figure 7d). The results confirmed former structural data and showed no significant variation of H-bond numbers upon binding to compound **4**. Average number of H-bonds per frame time (10 ps) were estimated as 122.97 ± 6.00 and 126.71 ± 6.54 for complex and apo conformation, respectively. Retaining a stable geometry could be further demonstrated by low CV value (4.88%) of intramolecular H-bonds in the complex form compared to the apo state (CV 5.16%).

SASA specifies an exterior area of protein that is exposed to the solvent molecules. On the basis of this definition, we were prompted to determine SASA fluctuations of the RhoA structure upon binding to compound **4** and its comparison with the apo form (Figure 8a). It was observed that SASA plots exhibited similar trends during MD simulations with average SASA values of 105.57 ± 2.65 (CV 2.51%) and 105.86 ± 2.32 (CV 2.19%) for the complex and apo states, respectively. No significant enhancement was observed in the RhoA SASA during MD simulations due to the lack of structural relaxation in complex and apo conformations.[60] According to the SASA distribution pattern, it might be deduced that the simulation time of 60 ns would be long enough for sampling equilibrated complexes. To get better insight into individual role of RhoA residues, per-residue SASA fluctuation plot was also obtained for the RhoA structure. For this purpose, SASA deviation of each amino acid upon binding to compound **4** with regard to the apo form is shown in Figure 8b. In confirmation to RMSF results, higher SASA fluctuations

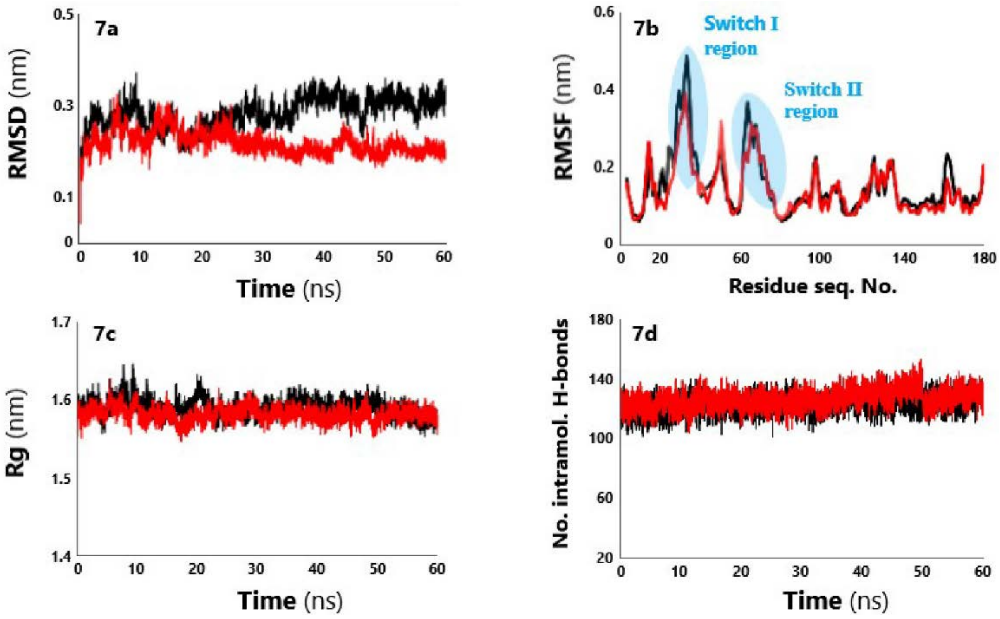

Figure 7. a) RMSDs of the backbone atoms of Homo sapiens RhoA upon binding to compound 4 (black) and in the apo form (red), b) RMSFs of the Cα atoms of Homo sapiens RhoA residues upon binding to compound 4 (black) and in the apo form (red), c) variation of the radius of gyration (Rg) of Homo sapiens RhoA in complex with compound 4 (black) and in the apo form (red) and d) variation of number of intramolecular H-bonds for Homo sapiens RhoA in complex with compound 4 (black) and in the apo form (red) during MD simulations (60 ns)

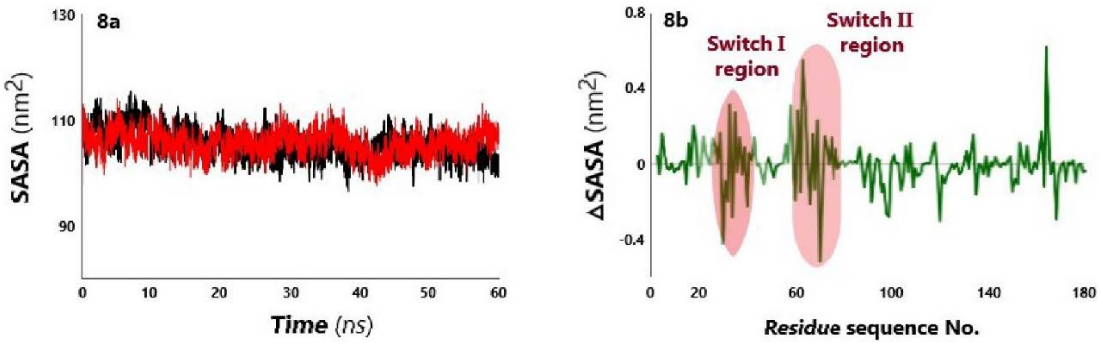

Figure 8. a) Solvent accessible surface area (SASA) of RhoA upon binding to compound 4 (blue), and in the apo form (red) and b) SASA difference (between complex and apo forms) for the amino acid residues of RhoA during the MD simulation period (60 ns)

were attributed to the residues of switch I and II regions. Our calculations demonstrated that Val33 (ΔSASA 0.315 nm^2) and Trp58 (ΔSASA 0.309 nm^2) moved to the more solvent exposed locations in the presence of compound **4**.[57]

Analysis of Small Molecule Structure

All atom RMSD variations of compound **4** indicated its persisted accommodation inside RhoA structure during MD simulations (CV 3.29%) (Figure 9a). In this regard, average RMSD was estimated to be 0.39 ± 0.01 nm. As depicted in Figure 9b, none of the heteroatoms of compound **4** showed RMSF values > 0.3 nm. The most fluctuated fragment of compound **4** was found to be a terminal phenyl ring (left side of the Figure 9b). This observation might be associated to the re-orientation of phenyl ring and its contribution to energy-favored hydrophobic contacts.

SASA values fluctuated approximately in the range of 4.10-5.66 nm^2 (Figure 9c). The average SASA value for compound **4** structure was estimated to be 4.88 ± 0.21 nm^2 (CV 4.48%) which is very close and comparable to the primary docked value (4.87 nm^2). We found that the RhoA-compound **4** complex was stabilized throughout hydrophobic contacts since average number of intermolecular H-bonds was estimated to be 0.06 ± 0.00 during MD time scale (Figure 9d). The H-bond plot showed that the intended complex formed one transient hydrogen bond that appeared mainly around 22 to 40 ns and disappeared afterward. In our opinion, lack of H-bond interaction(s) to RhoA structure might be attributed to the buried position of thiourea nitrogen atoms as the result of possible shifted rings towards the thiourea core.

Binding Conformation

Next step included a time-dependent calculation of the binding free energies between compound **4** and RhoA strucutres by a linear interaction energy (LIE) method.[61] For this purpose, average energies between compound **4** and its surroundings (Target and solvent) were estimated via MD binding trajectories (Figure 10).[62] As depicted in Figure 10, the intended complex was associated with stabilizing binding energies during the entire simulation time. The average bindig free energy was estimated to be -5.90 ± 0.04 kcal/mol. Our result was in good agreement with the mean binding energy of the docked complex (-5.42 kcal/mol). Short range van der Waals (Lennard-Jones) interaction energies (LJ-SR) for compound **4**-solvent association was obtained as -10.97 kcal/mol whereas; short range coulomb energy (Coul-SR) for compound **4**-solvent association was found to be -25.59 kcal/mol.

To understand the structural basis of the observed binding indices for RhoA-compound **4** complex, conformational trajectories were analyzed by trjconv functionality of GROMACS 5.1.1. For this purpose, various snapshots pertained to different time intervals were taken into consideration. Comparison of binding poses confirmed our previous results and revealed that compound **4** reoriented to attain its more stable conformation after about 25 ns. Extracted ligand-protein interaction patterns showed that the new conformation facilitated hydrophobic and electrostatic contacts to the RhoA residues (Figure 10). As estimated before, no stable H-bonds could be detected within the ligand protein interactions and it seemed that unlike the docked structure, shift of thiophene ring towards thiourea core put thiourea NH groups in a more buried position. In conformation to intermolecular H-bond plot (refer to Figure 9d), an unstable hydrogen bond interaction between Lys7 side chain NH and thiophene carbonyl oxygen of compound **4** tended to appear around 30 ns (Figure 10). Stable accommodation of compound **4** was evidenced by two hydrophobic interactions, one T-shaped π-stacking and a π-cation interaction. Compound **4** participated in π-cation interaction to The Lys7 sidechain amine group via thiophene ring. In this case, the distance between center

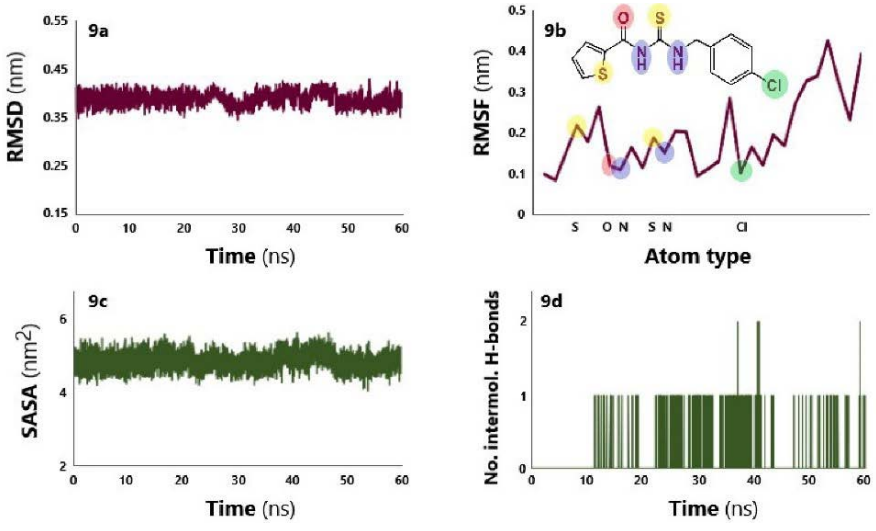

Figure 9. a) RMSD variations of compound 4 structure, b) RMSF variations of compound 4 atoms, c) variations of SASA for compound 4 structure and d) variation of number of intermolecular H-bonds between RhoA and compound 4 during MD simulation (60 ns)

of charge and aromatic ring center was estimated to be 4.49 Å. For the π-stacking, Trp58 pyrrole moiety and thiophene ring were interacted sites and distance between two ring centers was calculated to be 5.43 Å. Angle between two ring planes was estimated to be 85.49°. Asn41 and Asn43 were residues that contributed to two hydrophobic contacts to the carbon atoms of the phenyl ring. Within the interacted residues, Trp58 was merely belonged to the nucleotide binding site region and our characterized binding site that resided near the GTP binding pocket may offer more selectivity.[57] For more clarification, the main residues that were important in the interaction to compound **4** alongside their binding characteristics were summarized in Table 5. Obtained results showed that compound **4** could be accommodated near RhoA GTPase binding site and some interacted residues have been formerly reported in binding model of other inhibitors.[63] A major limitation of MD simulations is the timescale period. In this context, we tried to extend the simulation timescale up to the point that the achievement of stabilized binding patterns could be assured via its persistence in an acceptable period. All the binding indices were converged in the MD simulations but we plan to develop our computational facilities to extend the time for further studies.

Structure-Activity Relationship (SAR)

With regard to the number of synthetic derivatives, it would not be possible to offer a systematic SAR rules, but due to the similarity of the intended compounds with those of the previous researches by this group, it was tried to perform a few comparisons. The presence of EWGs on the aroyl ring increased the cytotoxic effect against AGS cells. As demonstrated in former studies,[64] there is a meaningful relation between electronegativity and cytotoxicity of carbonyl thiourea derivatives. The presence of chloro and nitro groups in compounds **11** and **12** led to the higher cytotoxicity with regard to other morpholine-based analogues. In this case, it might be probable that the electron-poor nature of the ring provided interactions with positively charged macromolecular targets. Besides highest cytotoxic effect of compound **4** against AGS cancer cells among other carbonyl thioureas, the MTT results indicated that it could not be considered as potent cytotoxic agent. Weak-cytotoxic inhibitors of cell migration may be prioritized anti-metastatic candidates over the cytostatic agents for their plausible more selective anti-metastatic effects. Results of the current study were correlated to a previous report on similar carbonyl thiourea derivatives.[24] It was demonstrated that some *N*1-substutued phenyl-*N*3-benzoyl thiourea derivatives without EWGs on benzoyl ring inhibited cell migration of various human cancer cell lines at doses insufficient to induce cell death.[65] Moreover; results of our previous studies revealed that dihydropyrimidine thiones which resembled the synthetic derivatives, showed higher inhibition of AGS cell migration when contained more hydrophobic rings.[66] This result could be relatively observed in the current carbonyl thiourea derivatives

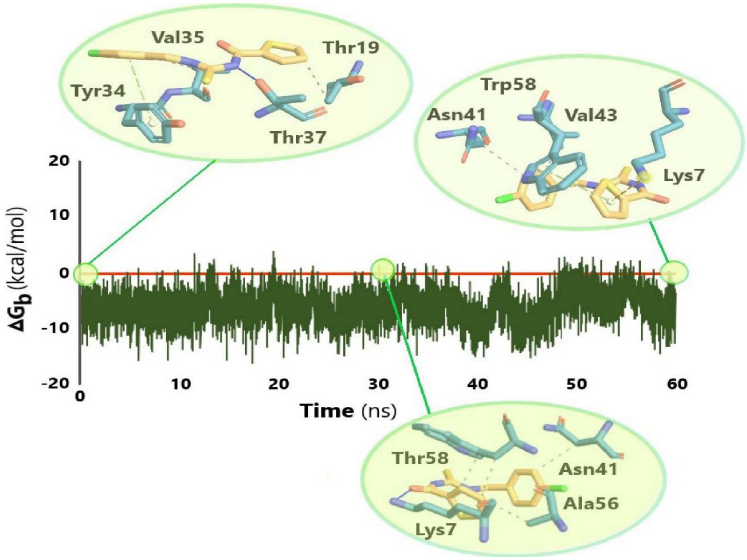

Figure 10. Free binding energies between RhoA structure and compound 4 during MD simulation (60 ns); Acquired binding conformations of compound 4 at different MD intervals (0, 30 and 60 ns) are designated

Table 5. Binding interactions and their characteristics between compound 4 and human RhoA GTP-binding site (PDB code: 5JHH) in the stable MD-driven complex

Interacted residue	Interaction type	Interacted residue atom	Interacted ligand atom	Bond length / distance (Å)
Lys7	π-cation	Side chain $^{+}NH_3$	Thiophene ring	4.49
Asn41	Hydrophobic	Side chain carbon	Phenyl carbon	3.77
Val43	Hydrophobic	Side chain alkyl	Phenyl carbon	3.50
Trp58	T-shape π-stacking	Side chain pyrrole ring	Thiophene	5.43

that included more hydrophobic characters. The results of molecular modeling studies gave some evidence on the presence of possible novel binding site near to the GTP-binding pocket. It was revealed that due to the presence of hydrophobic rings within the structure of compound **4**, it contributed to hydrophobic contacts with amino acid residues that have been previously observed in binding of other RhoA inhibitors.[63]

Conclusion

N1-(morpholin-4-ylethyl)/phenyl/aralkyl-*N3*-(thiophene-2-carbonyl)/benzoyl thiourea derivatives inhibited migration of AGS cells in wound-healing assay after 24 h at 6.25 µg/mL, and some derivatives such as **4** were observed to have comparable inhibition effects to *cis*-platin at even longer intervals. A comparison of the intended compounds with those of the previous researches indicated the increased cytotoxic effect against AGS cell lines as the result of benzoyl rings including EWGs. Although carbonyl thiourea derivatives with poor electron benzoyl rings are beneficial for developing anticancer agents, but our results specified that among the assessed derivatives, compound **4** may be an appropriate anti-metastatic candidate. In this context, future attempts may be focused on the development of compound **4** and similar structures since it may inhibit the migration of AGS cancer cells via metastatic mechanisms, without interference of cytotoxic effects.[19] Non-cytotoxic cell migration inhibitors such as **4** have advantage over the cytostatic agents as more selective anti-metastatic compounds. Results of this study could be to some extent correlated to a previous study that has been performed on *N*1-substutued phenyl-*N*3-benzoyl thiourea derivatives.[24] Miao et al., demonstrated a few *N*1-substutued phenyl-*N*3-benzoyl thiourea derivatives without EWGs on benzoyl ring to inhibit cell migration of various human cancer cell lines at doses insufficient to induce cell death.[65] Although the detailed binding modes of diverse carbonyl thiourea derivatives within corresponding target await further structural elucidations, molecular docking and dynamics simulations of compound **4** inside RhoA structure indicated the stability of ligand-protein complex (LIE free binding energy -5.90 kcal/mL). Our results differed a bit with previous reports on the MD-driven binding affinities of similar compound i.e. 1-(4-methoxybenzyl)-3-(4-methoxybenzoyl) thiourea as the top-scored inhibitor of AGS cancer cell migration (LIE free binding energy -6.54 kcal/mL). The results of MD simulations gave some evidence on the presence of possible novel binding site near to the GTP-binding pocket. It was revealed that compound **4** contributed in hydrophobic binding interactions with amino acid residues that have been formerly reported in binding model of other inhibitors.[63] In overall, acquired cell-based results and in silico evaluations suggested that compound **4** may be an appropriate candidate for future directions toward improving selective small molecule GTPase inhibitors against gastric cancer metastasis.

Acknowledgments

The research leading to offered results received funding from Ardabil University of Medical Sciences (ARUMS) under grant numbers IR.ARUMS.REC.1402.114 & IR.ARUMS.REC.1402.018.

Authors' Contribution

Conceptualization: Mohsen Sagha, Nima Razzaghi-Asl.
Data curation: Ghazaleh Rahgouy, Kosar Najafian, Jafar Abbasi Shiran.
Formal analysis: Ghazaleh Rahgouy, Narges Rajaei, Azadeh Aghvami Tehrani.
Investigation: Mohsen Sagha.
Methodology: Narges Rajaei.
Resources: Mohsen Sagha, Azadeh Aghvami Tehrani.
Supervision: Nima Razzaghi-Asl.
Writing–original draft: Nima Razzaghi-Asl.
Writing–review & editing: Mohsen Sagha.

Competing Interests

The authors declare no conflict of interests.

Ethical Approval

This study was approved by Research Ethics Committees of Ardabil University of Medical Sciences, Ethical codes: IR.ARUMS.REC.1402.114 and IR.ARUMS.REC.1402.018.

Funding

This study funded by Ardabil University of Medical Sciences, grant numbers: 401000044 and 401000075.

Supplementary Files

Supplementary files 1. AutoDock4.2 validation results for different 3D holo RhoA-ligand complexes retrieved from PDB
Supplementary files 2. MolSoft and SwissADME server data of the synthesized compounds
Supplementary file 3. Photographs of cell migration profile in DMSO

References

1. Thrift AP, Wenker TN, El-Serag HB. Global burden of gastric cancer: epidemiological trends, risk factors, screening and prevention. Nat Rev Clin Oncol. 2023;20(5):338-49. doi: 10.1038/s41571-023-00747-0.
2. Yoon J, Kim TY, Oh DY. Recent progress in immunotherapy for gastric cancer. J Gastric Cancer. 2023;23(1):207-23. doi: 10.5230/jgc.2023.23.e10.
3. Li H, Shen M, Wang S. Current therapies and progress in the treatment of advanced gastric cancer. Front Oncol. 2024;14:1327055. doi: 10.3389/fonc.2024.1327055.
4. Burz C, Pop V, Silaghi C, Lupan I, Samasca G. Prognosis and treatment of gastric cancer: a 2024 update. Cancers (Basel). 2024;16(9):1708. doi: 10.3390/cancers16091708.
5. Orditura M, Galizia G, Sforza V, Gambardella V, Fabozzi A, Laterza MM, et al. Treatment of gastric cancer. World J Gastroenterol. 2014;20(7):1635-49. doi: 10.3748/wjg.v20.i7.1635.
6. Smyth EC, Nilsson M, Grabsch HI, van Grieken NC, Lordick F. Gastric cancer. Lancet. 2020;396(10251):635-48. doi: 10.1016/s0140-6736(20)31288-5.
7. Jin G, Lv J, Yang M, Wang M, Zhu M, Wang T, et al. Genetic risk, incident gastric cancer, and healthy lifestyle: a meta-analysis of genome-wide association studies and prospective cohort study. Lancet Oncol. 2020;21(10):1378-86. doi: 10.1016/s1470-2045(20)30460-5.
8. Hui Y, Tu C, Liu D, Zhang H, Gong X. Corrigendum: Risk

factors for gastric cancer: a comprehensive analysis of observational studies. Front Public Health. 2023;11:1172663. doi: 10.3389/fpubh.2023.1172663.
9. Hu HM, Tsai HJ, Ku HY, Lo SS, Shan YS, Chang HC, et al. Survival outcomes of management in metastatic gastric adenocarcinoma patients. Sci Rep. 2021;11(1):23142. doi: 10.1038/s41598-021-02391-zhttps://doi.org/10.1038/s41598-021-02391-z.
10. Guan WL, He Y, Xu RH. Gastric cancer treatment: recent progress and future perspectives. J Hematol Oncol. 2023;16(1):57. doi: 10.1186/s13045-023-01451-3.
11. Dillekås H, Rogers MS, Straume O. Are 90% of deaths from cancer caused by metastases? Cancer Med. 2019;8(12):5574-6. doi: 10.1002/cam4.2474.
12. Lee JE, Kim KT, Shin SJ, Cheong JH, Choi YY. Genomic and evolutionary characteristics of metastatic gastric cancer by routes. Br J Cancer. 2023;129(4):672-82. doi: 10.1038/s41416-023-02338-3.
13. Lee M, Cho HJ, Park KS, Jung HY. ELK3 controls gastric cancer cell migration and invasion by regulating ECM remodeling-related genes. Int J Mol Sci. 2022;23(7):3709. doi: 10.3390/ijms23073709.
14. Raudenská M, Petrláková K, Juriňáková T, Leischner Fialová J, Fojtů M, Jakubek M, et al. Engine shutdown: migrastatic strategies and prevention of metastases. Trends Cancer. 2023;9(4):293-308. doi: 10.1016/j.trecan.2023.01.001.
15. Ye X, Weinberg RA. Epithelial-mesenchymal plasticity: a central regulator of cancer progression. Trends Cell Biol. 2015;25(11):675-86. doi: 10.1016/j.tcb.2015.07.012.
16. Lei ZN, Tian Q, Teng QX, Wurpel JN, Zeng L, Pan Y, et al. Understanding and targeting resistance mechanisms in cancer. MedComm (2020). 2023;4(3):e265. doi: 10.1002/mco2.265.
17. Ribatti D, Tamma R, Annese T. Epithelial-mesenchymal transition in cancer: a historical overview. Transl Oncol. 2020;13(6):100773. doi: 10.1016/j.tranon.2020.100773.
18. Wu JS, Jiang J, Chen BJ, Wang K, Tang YL, Liang XH. Plasticity of cancer cell invasion: patterns and mechanisms. Transl Oncol. 2021;14(1):100899. doi: 10.1016/j.tranon.2020.100899.
19. Akompong SK, Li Y, Gong W, Ye L, Liu J. Recently reported cell migration inhibitors: opportunities and challenges for antimetastatic agents. Drug Discov Today. 2024;29(3):103906. doi: 10.1016/j.drudis.2024.103906.
20. Widiandani T, Siswandono, Meiyanto E. Anticancer evaluation of N-benzoyl-3-allylthiourea as potential antibreast cancer agent through enhances HER-2 expression. J Adv Pharm Technol Res. 2020;11(4):163-8. doi: 10.4103/japtr.JAPTR_77_20.
21. Kesuma D, Siswandono, Purwanto BT, Rudyanto M. Synthesis and anticancer evaluation of N-benzoyl-N′-phenyltiourea derivatives against human breast cancer cells (T47D). J Chin Pharm Sci. 2019;29(2):123-9. doi: 10.5246/jcps.2020.02.010.
22. Ghorab MM, El-Gaby MS, Alsaid MS, Elshaier Y, Soliman AM, El-Senduny FF, et al. Novel thiourea derivatives bearing sulfonamide moiety as anticancer agents through COX-2 inhibition. Anticancer Agents Med Chem. 2017;17(10):1411-25. doi: 10.2174/1871520617666170327153735.
23. Thanigaimalai P, Lee KC, Sharma VK, Joo C, Cho WJ, Roh E, et al. Structural requirement of phenylthiourea analogs for their inhibitory activity of melanogenesis and tyrosinase. Bioorg Med Chem Lett. 2011;21(22):6824-8. doi: 10.1016/j.bmcl.2011.09.024.
24. Miao B, Skidan I, Yang J, You Z, Fu X, Famulok M, et al. Inhibition of cell migration by PITENINs: the role of ARF6. Oncogene. 2012;31(39):4317-32. doi: 10.1038/onc.2011.593.
25. de Oliveira TD, Plutín AM, Luna-Dulcey L, Castellano EE, Cominetti MR, Batista AA. Cytotoxicity of ruthenium-N,N-disubstituted-N′-acylthioureas complexes. Mater Sci Eng C Mater Biol Appl. 2020;115:111106. doi: 10.1016/j.msec.2020.111106.
26. Tokalı FS, Taslimi P, Demircioğlu İH, Şendil K, Tuzun B, Gülçin İ. Novel phenolic Mannich base derivatives: synthesis, bioactivity, molecular docking, and ADME-Tox studies. J Iran Chem Soc. 2022;19(2):563-77. doi: 10.1007/s13738-021-02331-8.
27. AlRawashdeh S, Barakat KH. Applications of molecular dynamics simulations in drug discovery. Methods Mol Biol. 2024;2714:127-41. doi: 10.1007/978-1-0716-3441-7_7.
28. Khan A, Ahmad L, Raza F, Khan SA, Ali T. Editorial: the practical implication of clinical pharmacokinetics in drug development, pharmaceutical analysis, and clinical research. Front Pharmacol. 2023;14:1252030. doi: 10.3389/fphar.2023.1252030.
29. Sagha M, Afghah Mortazavi K, Abbasi Shiran J, Aghvami Tehrani A, Razzaghi-Asl N. New 1-arylmethyl-3-benzoyl/cyclopropanoyl thioureas as inhibitors of AGS cell line migration: synthesis, biological evaluation and molecular dynamics. J Mol Struct. 2024;1312(Pt 1):138621. doi: 10.1016/j.molstruc.2024.138621.
30. Chang HR, Nam S, Lee J, Kim JH, Jung HR, Park HS, et al. Systematic approach identifies RHOA as a potential biomarker therapeutic target for Asian gastric cancer. Oncotarget. 2016;7(49):81435-51. doi: 10.18632/oncotarget.12963.
31. Kim JH, Park S, Lim SM, Eom HJ, Balch C, Lee J, et al. Rational design of small molecule RHOA inhibitors for gastric cancer. Pharmacogenomics J. 2020;20(4):601-12. doi: 10.1038/s41397-020-0153-6.
32. van Meerloo J, Kaspers GJ, Cloos J. Cell sensitivity assays: the MTT assay. Methods Mol Biol. 2011;731:237-45. doi: 10.1007/978-1-61779-080-5_20.
33. Wang X, Decker CC, Zechner L, Krstin S, Wink M. In vitro wound healing of tumor cells: inhibition of cell migration by selected cytotoxic alkaloids. BMC Pharmacol Toxicol. 2019;20(1):4. doi: 10.1186/s40360-018-0284-4.
34. Daina A, Michielin O, Zoete V. SwissADME: a free web tool to evaluate pharmacokinetics, drug-likeness and medicinal chemistry friendliness of small molecules. Sci Rep. 2017;7:42717. doi: 10.1038/srep42717.
35. Daina A, Zoete V. A boiled-egg to predict gastrointestinal absorption and brain penetration of small molecules. ChemMedChem. 2016;11(11):1117-21. doi: 10.1002/cmdc.201600182.
36. Morris GM, Huey R, Lindstrom W, Sanner MF, Belew RK, Goodsell DS, et al. AutoDock4 and AutoDockTools4: automated docking with selective receptor flexibility. J Comput Chem. 2009;30(16):2785-91. doi: 10.1002/jcc.21256.
37. Sanner MF. Python: a programming language for software integration and development. J Mol Graph Model. 1999;17(1):57-61.
38. Salentin S, Schreiber S, Haupt VJ, Adasme MF, Schroeder M. PLIP: fully automated protein-ligand interaction profiler. Nucleic Acids Res. 2015;43(W1):W443-7. doi: 10.1093/nar/gkv315.
39. Adasme MF, Linnemann KL, Bolz SN, Kaiser F, Salentin S, Haupt VJ, et al. PLIP 2021: expanding the scope of the protein-ligand interaction profiler to DNA and RNA. Nucleic Acids Res. 2021;49(W1):W530-4. doi: 10.1093/nar/gkab294.
40. Lv Z, Wang R, Ma L, Miao Q, Wu J, Yan Z, et al. Crystal Structure of the Ternary Complex Between the Human RhoA, its Inhibitor and the DH/PH Domain of Human ARHGEF11. RCSB Protein Data Bank (RCSB PDB); 2016. doi: 10.2210/pdb5JHH/pdb.
41. Van Der Spoel D, Lindahl E, Hess B, Groenhof G, Mark AE, Berendsen HJ. GROMACS: fast, flexible, and free. J Comput Chem. 2005;26(16):1701-18. doi: 10.1002/jcc.20291.
42. Malde AK, Zuo L, Breeze M, Stroet M, Poger D, Nair PC, et al. An automated force field topology builder (ATB) and repository:

version 1.0. J Chem Theory Comput. 2011;7(12):4026-37. doi: 10.1021/ct200196m.
43. Schmid N, Eichenberger AP, Choutko A, Riniker S, Winger M, Mark AE, et al. Definition and testing of the GROMOS force-field versions 54A7 and 54B7. Eur Biophys J. 2011;40(7):843-56. doi: 10.1007/s00249-011-0700-9.
44. Parrinello M, Rahman A. Polymorphic transitions in single crystals: a new molecular dynamics method. J Appl Phys. 1981;52(12):7182-90. doi: 10.1063/1.328693.
45. Hess B, Bekker H, Berendsen HJ, Fraaije JG. LINCS: a linear constraint solver for molecular simulations. J Comput Chem. 1997;18(12):1463-72. doi: 10.1002/(sici)1096-987x(199709)18:12<1463::aid-jcc4>3.0.co;2-h.
46. Darden T, York D, Pedersen L. Particle mesh Ewald: an N·log(N) method for Ewald sums in large systems. J Chem Phys. 1993;98(12):10089-92. doi: 10.1063/1.464397.
47. Bondi A. van der Waals volumes and radii. J Phys Chem. 1964;68(3):441-51. doi: 10.1021/j100785a001.
48. Ibrahim MA, Yusof MS, Amin NM. Anti-amoebic properties of carbonyl thiourea derivatives. Molecules. 2014;19(4):5191-204. doi: 10.3390/molecules19045191.
49. Duarte AB, Perez-Castillo Y, Andrade PN, de Castro RD, de Sousa DP. 3,5-Dinitrobenzoate and 3,5-dinitrobenzamide derivatives: mechanistic, antifungal, and in silico studies. J Chem. 2022;2022(1):2336175. doi: 10.1155/2022/2336175.
50. Mamedov VA, Zhukova NA, Voloshina AD, Syakaev VV, Beschastnova TN, Lyubina AP, et al. Synthesis of morpholine-, piperidine-, and N-substituted piperazine-coupled 2-(benzimidazol-2-yl)-3-arylquinoxalines as novel potent antitumor agents. ACS Pharmacol Transl Sci. 2022;5(10):945-62. doi: 10.1021/acsptsci.2c00118.
51. Sheikh AS, Altaf R, Nadeem H, Khan MT, Murtaza B. Formation of morpholine-acetamide derivatives as potent anti-tumor drug candidates: pharmacological evaluation and molecular docking studies. Heliyon. 2023;9(11):e22183. doi: 10.1016/j.heliyon.2023.e22183.
52. Roman R, Pintilie L, Căproiu MT, Dumitrașcu F, Nuță DC, Zarafu I, et al. New N-acyl thiourea derivatives: synthesis, standardized quantification method and in vitro evaluation of potential biological activities. Antibiotics (Basel). 2023;12(5):807. doi: 10.3390/antibiotics12050807.
53. Saeed A, Erben MF, Flörke U. Effect of fluorine substitution on the crystal structures and vibrational properties of phenylthiourea isomers. J Mol Struct. 2010;982(1):91-9. doi: 10.1016/j.molstruc.2010.08.012.
54. Prabhavathi H, Dasegowda KR, Renukananda KH, Lingaraju K, Naika HR. Exploration and evaluation of bioactive phytocompounds against BRCA proteins by in silico approach. J Biomol Struct Dyn. 2021;39(15):5471-85. doi: 10.1080/07391102.2020.1790424.
55. Badgwell DB, Lu Z, Le K, Gao F, Yang M, Suh GK, et al. The tumor-suppressor gene ARHI (DIRAS3) suppresses ovarian cancer cell migration through inhibition of the STAT3 and FAK/Rho signaling pathways. Oncogene. 2012;31(1):68-79. doi: 10.1038/onc.2011.213.
56. Zhang Y, Yan J, Xu H, Yang Y, Li W, Wu H, et al. Extremely low frequency electromagnetic fields promote mesenchymal stem cell migration by increasing intracellular Ca2+and activating the FAK/Rho GTPases signaling pathways in vitro. Stem Cell Res Ther. 2018;9(1):143. doi: 10.1186/s13287-018-0883-4.
57. Ortiz-Sanchez JM, Nichols SE, Sayyah J, Brown JH, McCammon JA, Grant BJ. Identification of potential small molecule binding pockets on Rho family GTPases. PLoS One. 2012;7(7):e40809. doi: 10.1371/journal.pone.0040809.
58. Jiang H, Zu S, Lu Y, Sun Z, Adeerjiang A, Guo Q, et al. A RhoA structure with switch II flipped outward revealed the conformational dynamics of switch II region. J Struct Biol. 2023;215(2):107942. doi: 10.1016/j.jsb.2023.107942.
59. Lin Y, Lu S, Zhang J, Zheng Y. Structure of an inactive conformation of GTP-bound RhoA GTPase. Structure. 2021;29(6):553-63.e5. doi: 10.1016/j.str.2020.12.015.
60. Damjanović A, Brooks BR, García-Moreno B. Conformational relaxation and water penetration coupled to ionization of internal groups in proteins. J Phys Chem A. 2011;115(16):4042-53. doi: 10.1021/jp110373f.
61. Aqvist J, Marelius J. The linear interaction energy method for predicting ligand binding free energies. Comb Chem High Throughput Screen. 2001;4(8):613-26. doi: 10.2174/1386207013330661.
62. Aqvist J, Luzhkov VB, Brandsdal BO. Ligand binding affinities from MD simulations. Acc Chem Res. 2002;35(6):358-65. doi: 10.1021/ar010014p.
63. Shang X, Marchioni F, Sipes N, Evelyn CR, Jerabek-Willemsen M, Duhr S, et al. Rational design of small molecule inhibitors targeting RhoA subfamily Rho GTPases. Chem Biol. 2012;19(6):699-710. doi: 10.1016/j.chembiol.2012.05.009.
64. Saeed S, Rashid N, Jones PG, Ali M, Hussain R. Synthesis, characterization and biological evaluation of some thiourea derivatives bearing benzothiazole moiety as potential antimicrobial and anticancer agents. Eur J Med Chem. 2010;45(4):1323-31. doi: 10.1016/j.ejmech.2009.12.016.
65. Miao B, Skidan I, Yang J, Lugovskoy A, Reibarkh M, Long K, et al. Small molecule inhibition of phosphatidylinositol-3,4,5-triphosphate (PIP3) binding to pleckstrin homology domains. Proc Natl Acad Sci U S A. 2010;107(46):20126-31. doi: 10.1073/pnas.1004522107.
66. Sagha M, Mousaei F, Salahi M, Razzaghi-Asl N. Synthesis of new 2-aminothiazolyl/benzothiazolyl-based 3,4-dihydropyrimidinones and evaluation of their effects on adenocarcinoma gastric cell migration. Mol Divers. 2022;26(2):1039-51. doi: 10.1007/s11030-021-10229-z.